

Characterization of Cement Minerals, Cements and their Reaction Products at the Atomic and Nanoscale Level

Jørgen Skibsted¹ and Christopher Hall²

¹ *Instrument Centre for Solid-State NMR Spectroscopy, Department of Chemistry, The University of Aarhus, DK-8000 Aarhus C, Denmark*

² *School of Engineering & Electronics and Centre for Materials Science & Engineering, The University of Edinburgh, Edinburgh EH9 3JL, UK*

1. Introduction

It is striking when we today survey the characterization scene on the atomic/nanoscale level how dominant X-ray diffraction and solid-state NMR methods remain. This could equally have been said 15 years ago. Other techniques appear in the sky from time to time and shine brightly, but rarely for long.

Of course we should remember how closely the development of cement science and especially of cement chemistry has always been intertwined with these two techniques. George Pake's paper [1] on the solid-state proton (¹H) NMR spectrum of gypsum was published in 1948 (one of us remembers reading it as an undergraduate), in the first decade of NMR research. This paper showed how the fine-structure of the ¹H NMR spectrum could provide a good estimate of the proton-proton distance to complement the X-ray crystal structure. The combined use of diffraction and NMR remains as valuable today: we can give as an example (one of several) the recent work of Hartman *et al.* [2] on the thermal decomposition of ettringites in which complementary time of flight neutron diffraction data and ¹H NMR spectra are beautifully integrated.

There is also the question: What is characterization? Is characterization the same as analysis? If not, what is it? A satisfactory definition is elusive. Here in the context of a conference on the chemistry of cements we take as our theme methods which allow us to identify, describe and distinguish the mineral components of cement (both individually and in whole cement) and their reaction products: this in a way that supports our most advanced understanding of the chemical behaviour of cement-based materials.

We shall devote most of this paper to diffraction and NMR techniques, (emphasising work reported in the last four years). Of other methods, we note that there is a surge of interest in Raman spectroscopy, and we therefore discuss the progress in this technique also. We shall offer some observations and speculations in conclusion.

2. X-ray diffraction for characterization

2.1 Rietveld analysis of cements

There is continuing development of Rietveld methods for the quantitative phase analysis of clinkers, whole cements and reaction product assemblages. Following the early initial work of J C Taylor *et al.* [3], a number of laboratories around the world are now reporting substantial studies, and round-robin exercises are published from time to time. Rietveld analysis of powder patterns from good quality laboratory diffractometers is becoming established as the method of choice for clinkers and cements, and indeed of materials such as slags and fly ashes. There are notable recent contributions from Peterson [4–6], Pritula *et al.* [7–9], Scarlett *et al.* [10], Stutzman [11], de la Torre *et al.* [12–15], and Walenta and Füllman [16–18]. These show the full gamut from on-line X-ray to synchrotron and neutron diffraction methods.

Successful Rietveld analysis demands good crystallographic descriptions of the minerals present, and for cements this is challenging because each of the clinker minerals has its own complexity. All are more or less heavily substituted and there are numerous polymorphs. Thus there is a continuing effort to better characterise the individual clinker phases: we note the work of Noirfontaine *et al.* [19] and Peterson [20,21] on polymorphs of alite, of Stephan and Wistuba [22] on C₃S solid solutions with MgO, Al₂O₃ and Fe₂O₃, and of Mori *et al.* [23] on polymorphs of belite.

While Rietveld quantitative phase analysis (QPA) of anhydrous clinkers and cements is driven principally by manufacturing quality control and standards interests, the Rietveld analysis of reaction products is emerging mainly to meet a research need. Rietveld analysis software is now readily available and its application to the characterization of hydration products, first reported by Scrivener *et al.* [24], is rapidly being taken up. Thus, Rivas Mercury *et al.* [25] have studied calcium aluminate cements with added silica, Meller *et al.* [26] hydrothermal CASH systems in which a large number of product phases are formed, while Christensen *et al.* [27] have investigated calcium aluminate hydration up to 170 °C.

Constraint by chemistry

It remains a matter of difficulty to establish independent measures of accuracy in QPA/QXRD for materials as complex as cements, both clinkers and production cements. Comparisons with the few reference materials available do not show spectacular agreement between Rietveld analyses and classical methods such as microscopic point-counting. Traditionally of course we depended greatly on the information provided by elemental (oxide) analysis, information which has the merit of being generally accurate. While the standard Bogue calculation is of no interest, much is now known about the partitioning of major and minor elements between the clinker phases and there is also a better understanding of the complex sulphate sub-system in cements. Using procedures such as proposed by Taylor [28,29] appears to yield results in close agreement with Rietveld analysis. The QPA in any case must be consistent with the known chemical composition and there are Rietveld analyses which either are not or are probably not consistent with even the major element composition of the cement. A single illustrative example of using XRD and chemical information together is provided in the characterisation of a Dyckerhoff oilwell cement [26]. For the main clinker phases the Rietveld and calculated modified-Bogue calculation are in good agreement. The modified-Bogue calculation however provides a large amount of supplementary information about the probable distribution of minor elements and also some detail about the probable mineralogy of the sulphate sub-system. In particular, it is useful to know the likely Al/Fe (A/F) ratio of the ferrite phase (in this case about 0.7), whether $\text{Ca}_3\text{Al}_2\text{O}_6$ (C_3A) is present or not (it is not and the two methods are in agreement); and what the Mg content of the ferrite is. Whether such information can be teased out of the Rietveld analysis alone is a question for the future.

The importance of applying chemical constraints or checks on QPA of product phases applies equally to hydration product assemblages. Thus there are usually more or less stringent stoichiometric constraints on what can be produced from a given set of starting materials. For example in a case reported by Meller *et al.* [26] the hydrothermal reaction of a low A/F cement with added silica under hydrothermal conditions produces xonotlite and gyrolite with some unreacted quartz. Rietveld analysis of the products is in excellent agreement with the stoichiometric constraint.

Particle size effects

We should add to this a caution also about particle size effects. Production cements have a very wide and asymmetric particle size distribution and it is known that the mineral composition varies strongly with particle size [30]. Thus interstitial phases are over-represented in the

finer fractions and the silicate phases in the coarser fractions. The sulphate minerals appear exclusively in the finest fractions. Since the coarser fractions generally have poor powder statistics, one may expect considerable sample to sample variation in the powder diffraction data of cements as-received, with the poorest reproducibility in the estimates of alite and belite content. A paper by Mitchell *et al.* [31] in this Congress presents valuable new results on particle size effects in Rietveld analysis.

2.2 New structures

X-ray and neutron diffraction continues to provide a steady flow of important information on the crystal structures of cement minerals and their reaction products. In the review period, there have been several notable examples which show clearly the steady improvement in data quality and the availability of the theoretical tools needed to deal with increasingly complex structures.

For example, there is the comprehensive single-crystal and powder X-ray diffraction study by Redhammer *et al.* [32] of the structure of the brownmillerites, $C_4A_xF_{2-x}$, as a function of A/F ratio and temperature. These brownmillerites show a structural phase transformation which occurs at about 730 °C in the pure Fe mineral and at lower temperatures as the Al content rises. This work is complemented to some extent by the study of Zötzl and Pöllmann [33] on Mn substitution in brownmillerites (relevant to the enhanced reactivity of Mn-containing calcium aluminate cements) and the synchrotron X-ray and neutron diffraction investigation by Jupe *et al.* [34] on the structural effects of the charge balancing Mg/Si substitution in brownmillerites which is known to occur significantly in clinker ferrite (importantly in oilwell cements). There is ever more evidence of the chemical and microstructural complexity of the ferrite phase, with wild swings in composition on short length scales [35], coupled with accompanying structural variations [36]. All these papers taken together point to an increasing interest in the effects of guest ions on structure and hence on reactivity of minerals. One should say also on morphology but that link has not yet been strongly forged.

Of studies on hydrates and other reaction product minerals, there are the exceptionally valuable recent structural investigations of jennite and of 14Å- tobermorite by Bonaccorsi [37,38¹] which of course bear on the central question of the structure of C-S-H. The jennite (Fig. 1) and tobermorite

¹ Hal Taylor's last published paper.

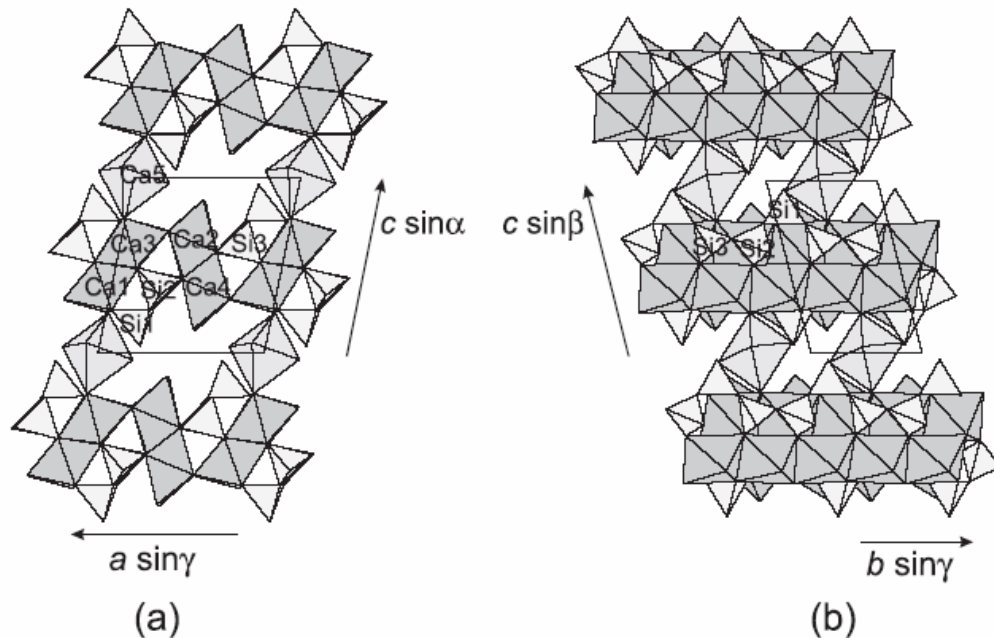


Fig. 1. Crystal structure of jennite as seen along (a) [010] and (b) [100]. Adapted from ref. [37].

structures are extremely challenging because of the existence of stacking disorder along 001 and solving them requires the use of order-disorder theory. These solutions continue the line of the earlier work on 11Å-tobermorite [39] and on polytypes of xonotlite by Hejny and Armbruster [40]. These intrinsic structural difficulties are exacerbated by the experimental difficulty of obtaining good single crystal samples, solved in both cases by the use of very small crystals on a synchrotron diffractometer. The refined structure of gypsum (Fig. 2) by de la Torre *et al.* [41] is an example of a trend towards the use of high-quality synchrotron X-ray diffraction powder data in preference to classical single-crystal methods for structure determination. Garbev describes structural studies of a number of hydrothermal silicate hydrates using Rietveld analysis in an unpublished thesis [42]. Among non-silicate hydrates, there is a continuing fascination with the subtle and fragile structure of ettringite. The importance of ettringite in cement chemistry is of course considerable, but its appeal lies also in its ease of synthesis and its rich thermal decomposition behaviour in the accessible range up to 120 °C. The excellent new structural study by Hartman and Berliner [43] using time-of-flight neutron diffraction data from deuterio-ettringite has been used as the basis of a straightforward Rietveld refinement of laboratory X-ray powder data by Goetz-Neunhoeffer and Neuberger [44] (Fig. 3). This structure includes positions of all water molecules and is a significant advance on the library structure from Moore and Taylor [45] which dates from 1973. From a

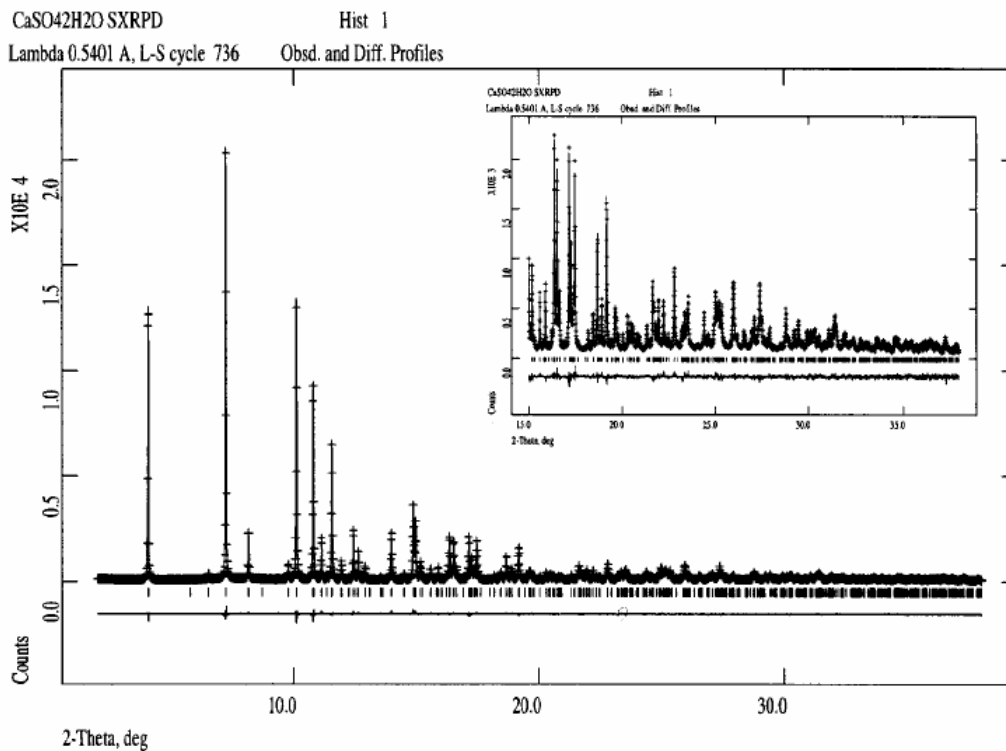


Fig. 2. Rietveld refinement of synchrotron X-ray powder diffraction data ($\lambda = 0.54 \text{ \AA}$) for $\text{CaSO}_4 \cdot 2\text{H}_2\text{O}$. The inset shows the high angle range of this pattern. Adapted from ref. [41].

characterization perspective, this is a clear step forward in understanding the behaviour of a complex hydrate (of which it is perhaps superfluous to say that there are many in cement chemistry). A whole new field of meta-hydrates is opening up, in which we see structural distress at the crystallographic level as loss of water molecules causes more or less severe lattice distortion preceding full-blown structural transformation. This is well illustrated not only by recent work on meta-ettringite [46] but also by the example of meta-jennite where the cause of shrinkage produced by progressive loss of water can now be understood essentially molecule by molecule, starting with the loss of coordination water from the Ca5 ion [38]. Bassanite ($\text{CaSO}_4 \cdot \frac{1}{2}\text{H}_2\text{O}$) is another such meta-hydrate which continues to attract attention.

This work on meta-hydrates is the first of several instances where characterisation shades into something else, as we see characterisation methods being applied *dynamically* to track transformations and reactions.

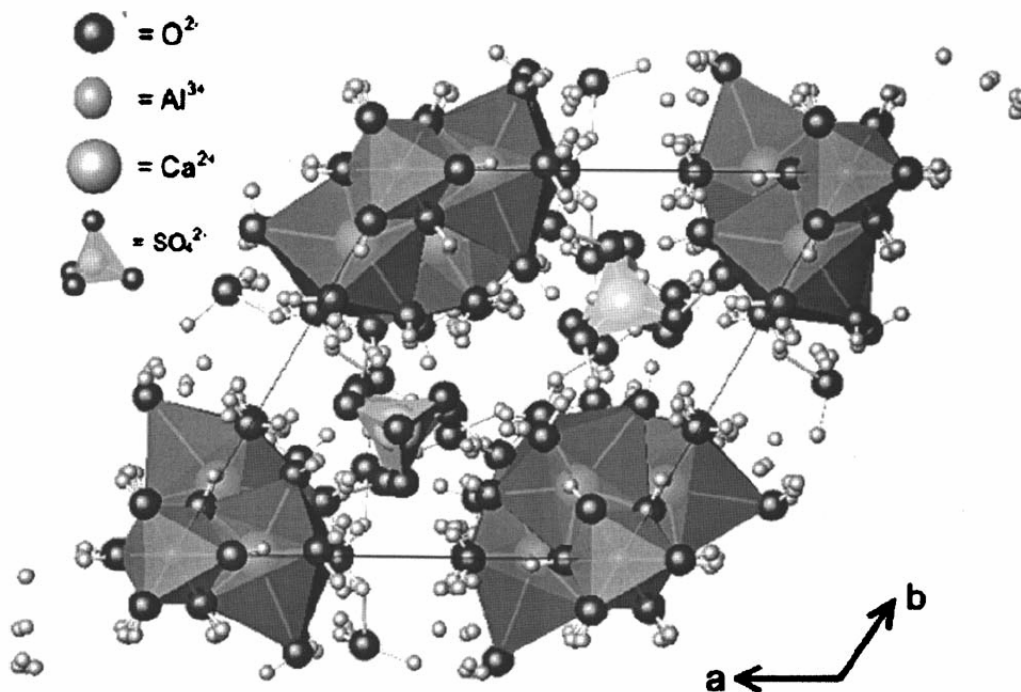


Fig. 3. Hexagonal unit cell of the revised crystal structure for ettringite projected along the *c* axis. Adapted from ref. [44].

2.3 Synchrotron advances

For some years now the vigorous development of X-ray methods has been largely if not wholly driven by synchrotron science [47]. We have already noted the frequent and growing use of synchrotron X-ray data in structural studies. Here the benefits of synchrotron methods lie mainly in the high source brilliance and collimated X-ray optics which can provide high resolution powder data or single-crystal data from small specimens. However the synchrotron brings other powerful opportunities, both in new ways of carrying out diffraction experiments and also in exploiting other phenomena for characterization. The synchrotron makes available a wide range of photon energies, from hard X-rays with great penetrating power to soft X-rays for microscopy (as well as visible and infra-red radiation). These light source characteristics when combined with developments in detector technology dramatically extend the possibilities. In particular, we can now achieve fine time-slicing in time-resolved diffraction; we can do diffraction mapping in complex bulk specimens to provide spatially-resolved diffraction (and indeed in principle can do both at the same time). We can in addition use various forms of X-ray absorption spectroscopy to provide new information on the chemical state of elements within samples. Finally we can combine wide-angle X-ray scattering, small-angle

scattering and spectroscopy in a single experiment to provide a stereo view of materials and processes. Cement chemistry already provides recent examples of many of these.

Time-resolved diffraction

The workhorse technique for more than a decade has been energy-dispersive diffraction with hard synchrotron X-rays (say at least 50 keV), allowing penetration of the X-ray beam through samples such as cement pastes 10–20 mm thick and acquisition times as short as 30 s. This instrumental arrangement is well (if not ideally) suited to identifying and tracking the transformations occurring in the hydration of single minerals and cements by fixed-angle diffraction [48]. Such hard X-rays can penetrate sample cans and pressure vessels, at least of modest wall thick-

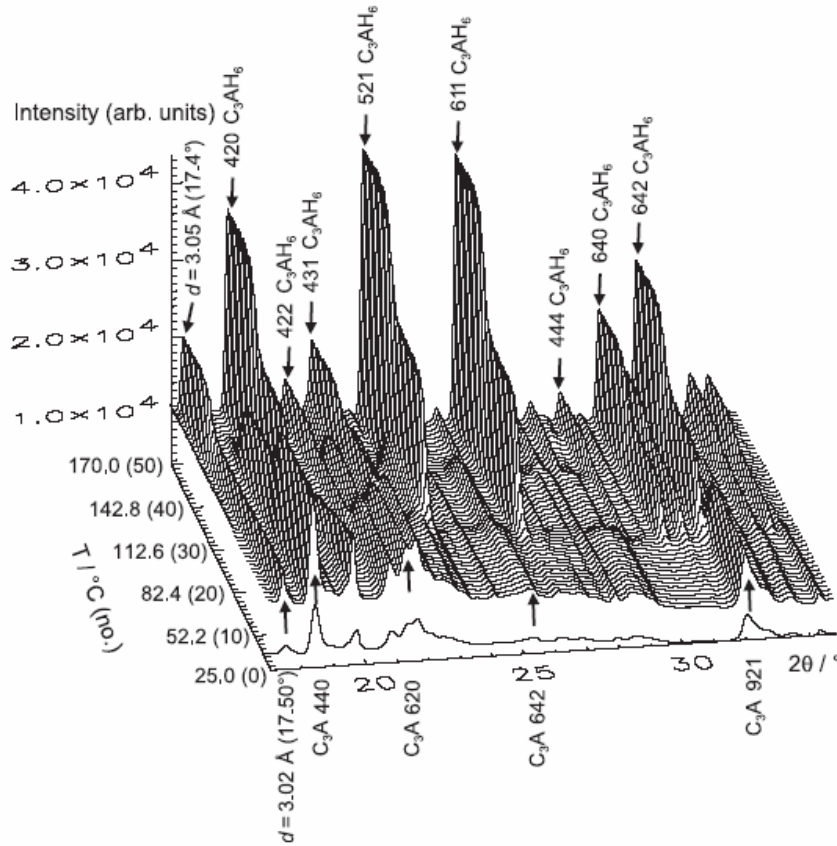


Fig. 4. Stack plot of powder patterns of a C_2AH_x/C_4AH_x mixture in the 2θ range 17.2° to 35° . Positions of C_3A reflections are marked with Miller indices for the first pattern recorded, and positions of the end product C_3AH_6 are marked with Miller indices. Adapted from ref. [49].

ness, so that hydrothermal conditions can be investigated up to say 300 °C. As an alternative to this arrangement, synchrotron angle-dispersive data can now be obtained quite rapidly using area detectors. The low photon energy requires the use of capillary samples but even so Christensen *et al.* [27] and Jensen *et al.* [49] (Fig. 4) and tracked hydration transformations up to 170 °C in calcium aluminate, tricalcium aluminate and portland cement systems. In these measurements glass or quartz capillaries were used, and the wet sample was pressurised at (typically) 40 bar with nitrogen gas to maintain liquid water in contact with the solid. The latest advances in this type of experimental configuration are to be found on the UK synchrotron RAPID system, where the novel multiwire detector provides at best millisecond data acquisition times (and routinely a few seconds) for a complete powder pattern with very high resolution. While this may not be required for most cement systems, it does allow very fine time-slicing of the fast transformations sometimes seen in hydrothermal systems. We show as one example the gypsum-bassanite-anhydrite sequence (Fig. 5), which incidentally reveals clearly a structural change in bassanite at around 140 °C [50], where water is lost easily and smoothly to form γ -anhydrite. This is another example of a meta-hydrate

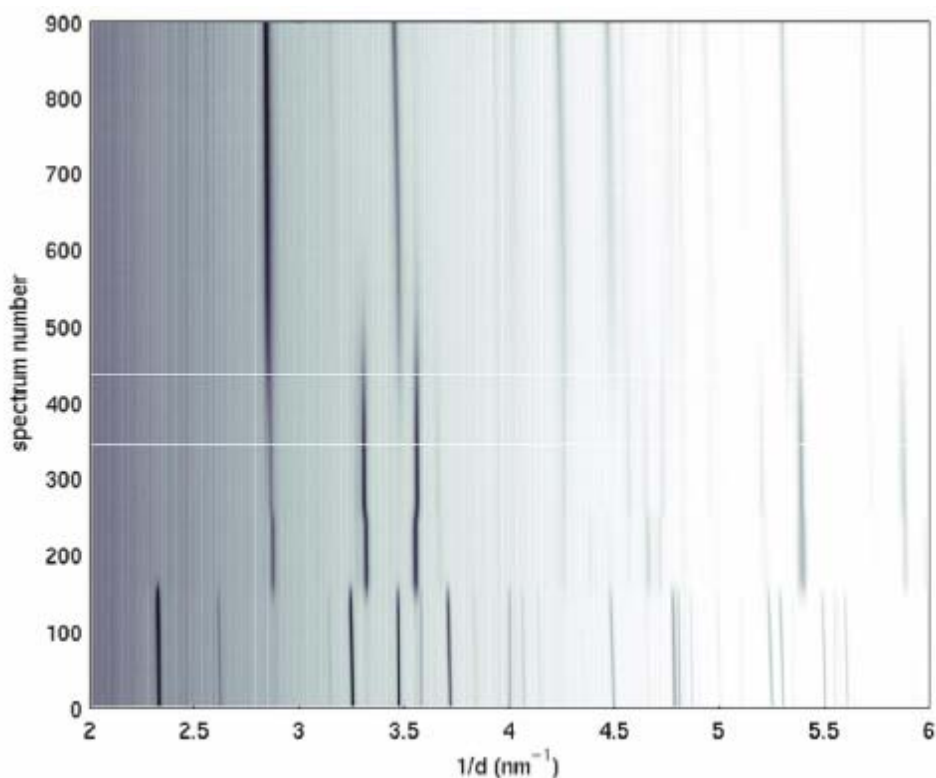


Fig. 5. Thermal transformation of gypsum to bassanite, gamma-anhydrite and anhydrite. Contour plot constructed from 900 diffraction patterns collected for 1s at 4s intervals over 1h. Adapted from ref. [50].

transformation and shows graphically the structural continuity between bassanite and γ -anhydrite. A second example is the ettringite-mono-sulphate-hydrogarnet sequence recently recorded by Meller (Fig. 6). Both these cases show that detailed structural characterisation can be obtained from in-situ time-resolved experiments. They also show the rapid transformations no doubt associated with nucleations and rapid crystal growth from solution.

Space-resolved diffraction

Spatially-resolved X-ray diffraction is also now possible using highly collimated synchrotron X-ray beam to probe a bulk specimen. The original TEDDI concept uses hard X-rays and collects powder diffraction data from a well-defined voxel within the specimen, typically a few mm^3 in volume. This is the first time that it has been possible to collect diffraction data from the interior of an extended heterogeneous material. An early application, so far rather under-exploited, is to use this for bulk averaging of composition without sample preparation. True spatial mapping, first applied to sedimentary rocks, has been reported for carbonation of

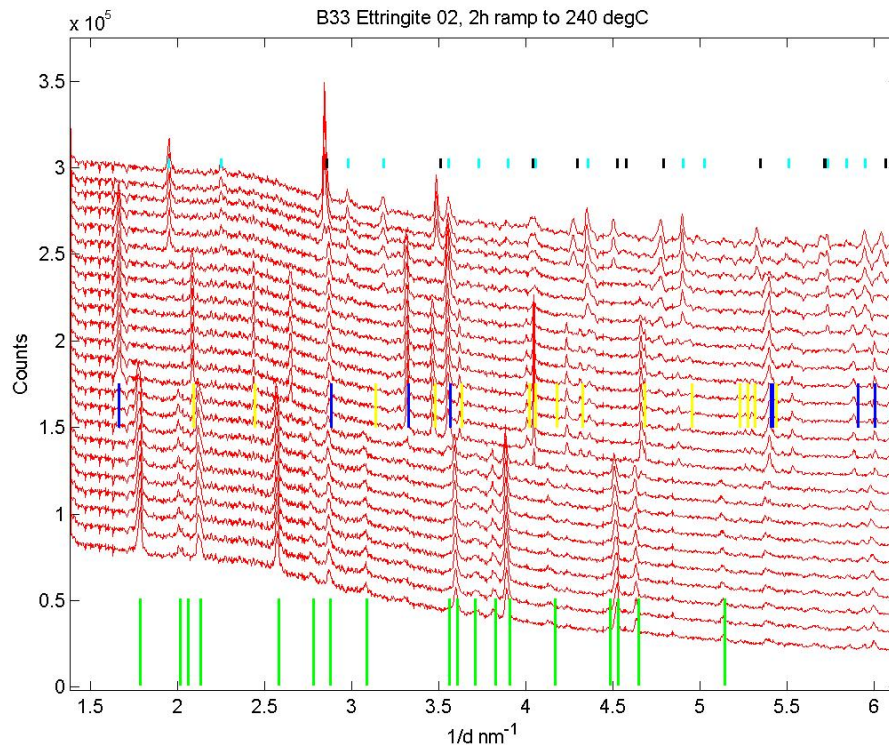


Fig. 6. Thermal decomposition of ettringite producing successively AFm-14 + bassanite, and katoite hydrogarnet and anhydrite (Meller & Hall 2007, unpublished).

cements. However, the real potential of diffraction imaging awaits a more efficient data acquisition process. Recently, Tunna *et al.* [51] describe a new laser machined 2D collimator array which will allow simultaneous data acquisition from 256 voxels. The collimator, whose fabrication demands extremely high precision, is matched to a new energy-dispersive detector array.

There is no reason in principle why space- and time-resolved studies should not be combined. This has not yet been done for any cement-based systems, but there are examples from related areas.

Strain measurements

One exciting application of diffraction mapping through large specimens is in obtaining strain distributions. This brings together chemistry and mechanics. Strains may either be locked-in strains (from clinkering processes or from confined crystal growth during hydration or from reaction damage), or else from external forces. Facilities for examining and characterising engineering materials (even engineering components) will be increasingly available in synchrotron laboratories as engineering and materials become increasingly the focus of their work. Steuwer *et al.* [52] show what can be done with present techniques applied to metal alloys, and Biernacki *et al.* [53] bring these methods directly to bear on cement pastes, in effect using portlandite crystals as a micro strain gauge within the hardened material. Strains of 1×10^{-5} can be resolved. In this case, the strain distribution was not mapped but with enhanced TEDDI methods this should soon become possible. Benedikt *et al.* [54] show that small particles such as aluminium may be deliberately dispersed within a material for a similar purpose, a scheme not yet used in cement materials.

Extreme conditions

Clinkers are formed under extreme kiln conditions and many hydrated cements and concretes have to perform under severe service environments. We note therefore the considerable activity in techniques for *in-situ* observation of materials in tests where we can impose high temperatures, high pressures or aggressive chemical environments (or indeed all three). A spectacular example at high temperature is the synchrotron diffraction (strictly, small-angle scattering) to observe short-range structure in a glassy form of monocalcium aluminate (CA) at high temperatures. This was achieved by an experimental arrangement in which the sample was fused by laser heating and levitated on a gas plume: a sample without a container. Such methods have clear general application to the exploration of clinkering reactions. At the other extreme, synchrotron furnace devices now allow capillary samples to be studied to

temperatures of at least 800 °C and hydrothermal systems to at least 250 °C [55].

3. X-ray absorption spectroscopy

Synchrotron X-ray sources also allow the detection and speciation of elements by means of their absorption spectra, X-rays being absorbed through excitation of electrons. Absorption edges occur at characteristic energies for each element, and analysis of the fine-structure near the absorption edge provides information on the short-range environment of the absorbing element and its oxidation state, in other words its speciation. XAS in its several implementations go by the acronyms EXAFS/XANES/NEXAFS. For many elements, XAS has high sensitivity (detection limits of tens of ppm) so that it is especially useful in detecting and speciating minor or trace element species in cement systems. Thus

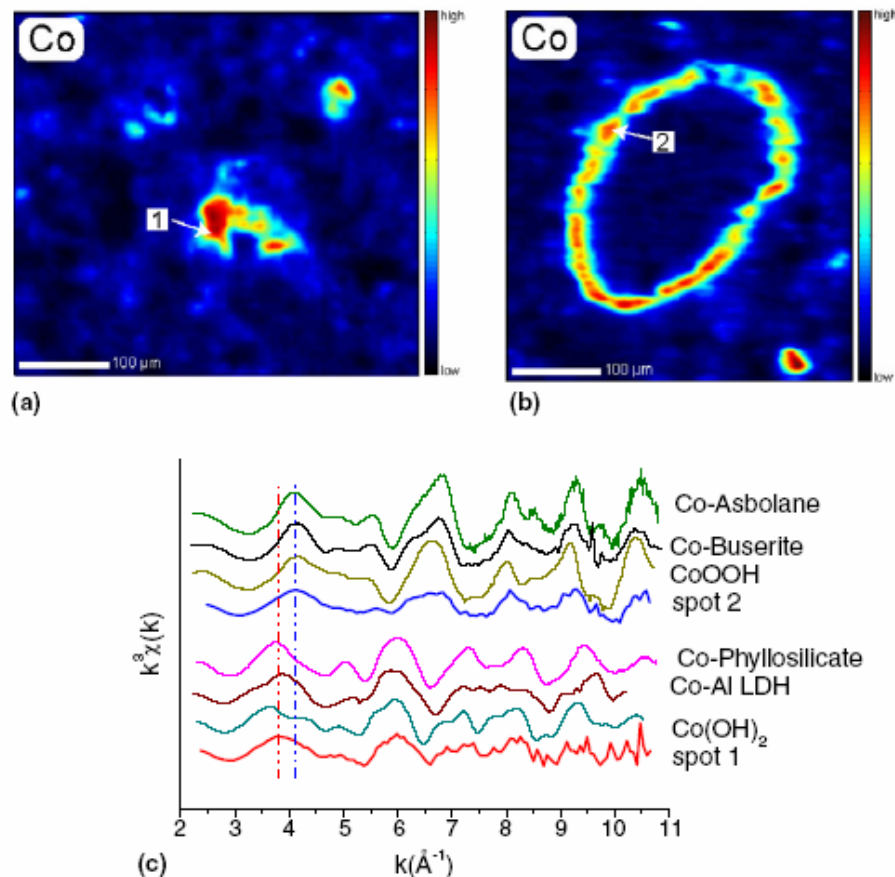


Fig 7. Elemental Co distribution map of a Co-doped cement sample hydrated for 3 days: (a) Co-rich spot 1; (b) Co-rich spot 2; (c) k^3 -weighted, normalized, background-subtracted Co K-edge XAS spectra collected at spot 1 and 2 in comparison with the spectra of Co reference compounds. Adapted from ref. [56].

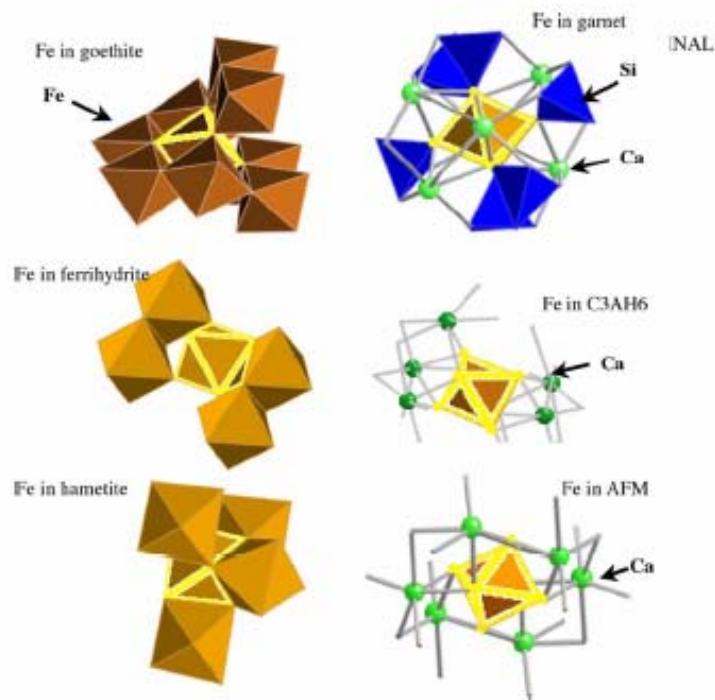


Fig. 8. Atomic environment around Fe in different Fe minerals. Adapted from ref. [58].

applications of XAS in cement characterization – while not numerous – cluster around heavy metal immobilization. A useful review is provided by Scheidegger *et al.* [56] in relation to studies of Sn and Co incorporation into C-S-H (Fig. 7); and a further study deals with the incorporation of Ni in cement systems [57]. XAS may also provide information on minor cement elements: for example, on the fate of Fe in cement hydration (Fig. 8) [58]. Jupe *et al.* also EXAFS to complement X-ray diffraction data in determining the site occupancy of this element in brownmillerites [34].

4. Multi-techniques The only limit to combining a variety of these techniques into a single experiment is practical ingenuity. For example, in the field of zeolite synthesis, Beale *et al.* [59] show how X-ray diffraction, SAXS and X-ray absorption spectroscopy may be used together to observe the nucleation of template zeolite nanocrystals at the 10 nm scale and their subsequent growth aggregation and structural development. In this case, the microporous solid phase contained Zn which was observed by EXAFS. There is no doubt that such an approach could bring rich pickings in cement science, as a characterization of scale on several length scales and involving both amorphous and crystalline components.

5. Nuclear magnetic resonance spectroscopy

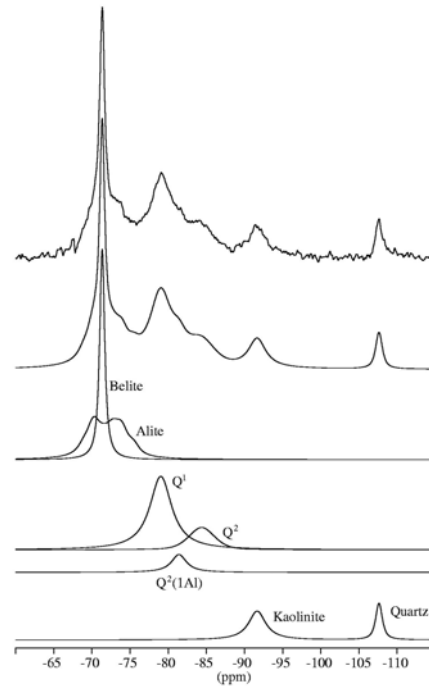
NMR techniques have been increasingly employed in studies of cementitious materials over the last three decades [60–62]. The main advantages of the basic method is the nuclear-spin selectivity, where only one nuclear-spin isotope of the NMR periodic table (e.g., ^1H , ^{19}F , ^{27}Al , ^{29}Si , ^{35}Cl) is detected at a time, and the fact that the resonances from these spins reflect local structure and/or dynamic effects. Thus, amorphous and crystalline phases are equally detected, thereby complementing diffraction techniques which probe long-range. The applications of NMR in cement science fall roughly in three types of quite different approaches, which employ specific nuclear-spin properties of the spins present in cements. High-resolution magic-angle spinning (MAS) NMR of dry, powdered samples generally utilizes the reflection of the local electronic structure in the isotropic chemical shift (δ) to provide quantitative and structural information about the environments for spins such as ^{29}Si and ^{27}Al in the anhydrous and hydrated phases of Portland cements. Another approach takes advantage of the high sensitivity of the ^1H isotope in experiments which utilize that the relaxation rates ($1/T_1$ and $1/T_2$) change significantly in the vicinity of solid-liquid interfaces and thereby can provide information about porosity, pore-size distributions and interconnectivities. Finally, spatially-resolved NMR (i.e., magnetic resonance imaging, MRI) has been employed, where magnetic field gradients superimposed on the static field provide a frequency-encoding of the NMR signal that can be related to the spatial position of the spins in the sample. MRI is mainly applicable to studies on the μm – mm level and thereby useful in the characterization of pores, cracks, and water diffusion on that scale. However, MRI techniques will not be described in this review where the following two sections will focus on high-resolution NMR and ^1H relaxation-time analyses.

5.1 High-resolution Magic-Angle Spinning NMR

Despite the low natural abundance for ^{29}Si (4.7 %) and its generally long relaxation times, resulting in long experiment times, ^{29}Si MAS NMR represents still one of the most popular NMR tools in studies of Portland cements. The spectroscopic features of the ^{29}Si MAS NMR spectra for the anhydrous components, alite, belite, and several admixtures (e.g., quartz, silica fume, metakaolin) as well as for the basic structure of the C-S-H phase are well established [60–62]. This knowledge has been utilized in studies of the hydration kinetics for the alite and belite phases in Portland cements including various additives or supplementary cementitious materials. As an example, a ^{29}Si MAS NMR investigation of mixtures of white Portland cement and the clay minerals kaolinite ($\text{Al}_2\text{Si}_2\text{O}_5(\text{OH})_4$, Fig. 9) and bentonite ($\text{M}_{x+y}((\text{Al},\text{Fe})_{2-x}\text{Mg}_x)(\text{Si}_{4-y}\text{Al}_y)\text{O}_{10}(\text{OH})_2$, $\text{M} = \text{Na}^+$, K^+ , Ca^{2+})

has shown that both clays accelerate the hydration for alite and belite most likely because the finely dispersed clay particles act as nucleation agents for the formation of the C-S-H phase [63]. Furthermore, the separate observation of the ^{29}Si resonance from kaolinite (-91.5 ppm, Q^3 units) in the hydrated samples revealed that the basic structure of kaolinite is not affected by the alkaline medium of the hydrating cement and thereby the absence of any pozzolanic reactions for kaolinite.

Fig. 9. ^{29}Si MAS NMR spectrum (7.1 T, $\nu_R = 7.0$ kHz) of a white Portland cement – kaolinite mixture (4:1 w/w) hydrated for 2 days. Below the experimental spectrum is shown the optimized deconvolution along with sub-spectra of the individual silicate components including a quartz impurity from the kaolinite additive. Adapted from ref. [63].



Recently, it has also been shown that valuable information about the incorporation of Al in the C-S-H phase formed in hydrating Portland cement can be obtained from ^{29}Si MAS NMR. Generally, these spectra allow observation of resonances from the Q^1 , Q^2 , and $\text{Q}^2(1\text{Al})$ sites (Fig. 10) of the silicate chains in the C-S-H structure [64,65]. Thus, the different types of Q^2 sites, i.e. the paired SiO_4 chain sites (Q_B^2) and the bridging Si sites (Q_B^2), can not be distinguished by ^{29}Si MAS NMR for C-S-Hs resulting from Portland cement hydration. However, the average chain length of alumino-silicate tetrahedra ($\overline{\text{CL}}$), of pure SiO_4 units ($\overline{\text{CL}}_{\text{Si}}$), and the degree of Al substitution in the tetrahedral chains ($\text{Al}_{\text{IV}}/\text{Si}$) can be obtained from the intensities of the Q^1 , Q^2 , and $\text{Q}^2(1\text{Al})$ resonances, employing the formulas [66,67]:

$$\overline{\text{CL}} = \frac{2[\text{Q}^1 + \text{Q}^2 + \frac{3}{2}\text{Q}^2(1\text{Al})]}{\frac{1}{2}\text{Q}^1} \quad \overline{\text{CL}}_{\text{Si}} = \frac{\text{Q}^1 + \text{Q}^2 + \text{Q}^2(1\text{Al})}{\frac{1}{2}(\text{Q}^1 + \text{Q}^2(1\text{Al}))} \quad (1)$$

$$\text{Al}_{\text{IV}}/\text{Si} = \frac{\frac{1}{2}\text{Q}^2(1\text{Al})}{\text{Q}^1 + \text{Q}^2 + \text{Q}^2(1\text{Al})} \quad (2)$$

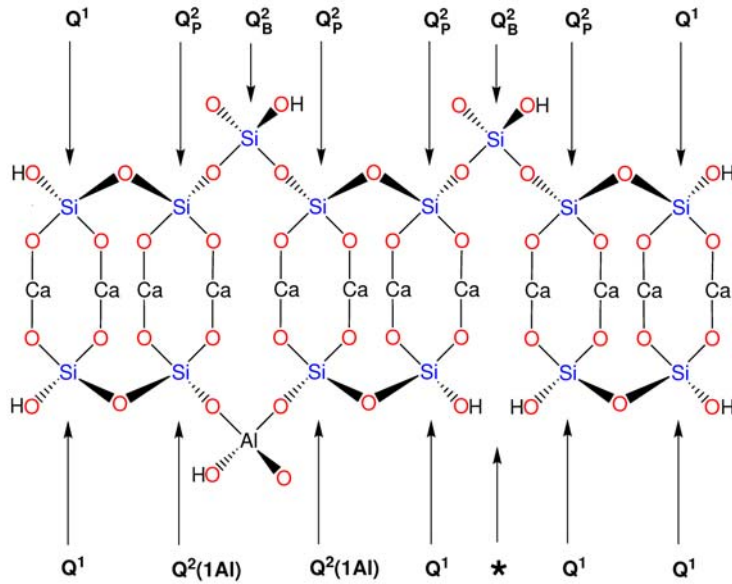


Fig. 10. Schematic representation of the basic structural unit of the C-S-H phase. The layer of seven-fold coordinated Ca is sandwiched inbetween “dreierketten” chains of SiO_4 tetrahedra. The upper part shows an octameric silicate chain while the lower part illustrates the incorporation of Al in a bridging site and a defect site (*) in the silicate chain structure.

These measures have been used to study the incorporation of Al in the C-S-H phase resulting from hydration of a white Portland cement, where the quantity of Al^{3+} ions in solution was increased by hydrating the cement in 0.3 and 0.5 M solutions of NaAlO_2 [67]. From the indirect detection by ^{29}Si MAS NMR of tetrahedrally coordinated aluminium (Al_{IV}) in the C-S-H, it was found that the $\text{Al}_{\text{IV}}/\text{Si}$ ratio for the C-S-H is almost independent of the hydration time but increases with increasing amount of Al^{3+} ions available in the solution, i.e., average $\text{Al}_{\text{IV}}/\text{Si}$ ratios of 0.042, 0.064, and 0.083 were determined for the white Portland cement hydrated in water and in 0.3 M and 0.5 M NaAlO_2 solutions, respectively [67]. Furthermore, an evaluation of the average tetrahedral chain lengths showed that the $\text{AlO}_4\text{-SiO}_4$ chain lengths increase with increasing hydration time and increasing concentration of aluminate species in the solutions. On the contrary, the chain lengths of pure silicate tetrahedra are almost independent on the concentration of Al^{3+} ions in the solutions. These observations suggest that Al^{3+} ions, most likely in the form of $\text{Al}(\text{OH})_4^-$ ions, link together already existing polymeric silicate chains, thereby forming aluminosilicate chains with longer average chain lengths [67]. This mechanism for incorporation of Al in the C-S-H suggests that the Al^{3+} ions act as a linker for silicate chains that have already been formed. Moreover, the mechanism agrees well with results by Richardson and Groves [66] which strongly indicate that Al_{IV} only occupies bridging chain sites in the C-S-H structure.

An increased amount of Al in the cement mixture, introduced by addition of metakaolin (“Al₂Si₂O₇”), may also result in a significant increase in the Al_{IV}/Si ratio for the C-S-H as shown by Love *et al.* [68] in a ²⁷Al, ²⁹Si MAS NMR and TEM study of a white Portland cement – metakaolin mixture (4.1 w/w) hydrated in water and in a 5.0 M KOH solution. From ²⁹Si MAS NMR they observed an increase in Al_{IV}/Si from 0.06 to 0.24 and in \overline{CL} from 2.8 to 11.0 for samples hydrated in water for 1 day and 28 days, respectively. Even higher values for both parameters at the same hydration times were observed for the KOH-activated samples and reflect an increased degree of reaction for the metakaolin admixture caused by alkali activation. The values for the mixture hydrated for 28 days in water correspond to a C-S-H which on average includes 11 tetrahedral units in the chains and with two of the three bridging sites occupied by Al (e.g. Q_B², Fig. 10). Thus, a significant amount of the aluminium released by the pozzolanic reaction of metakaolin is incorporated in the C-S-H. Moreover, the alkali activation results in significant smaller linewidths of the resonances from the SiO₄ sites in the C-S-H [68], demonstrating a higher degree of local structural order for the C-S-H prepared by this method.

The overlap of resonances in studies of binary Portland cement systems containing slag has been addressed by Dyson *et al.* [69] using ²⁹Si MAS NMR combined with selective dissolution techniques. Generally, slags exhibit very broad ²⁹Si peaks, which may extend over the full chemical shift range for SiO₄ sites, i.e., –60 ppm to –120 ppm. As a first approach, the ²⁹Si MAS spectra may be analyzed using a simulated sub spectrum of the anhydrous slag in addition to sub spectra for alite, belite, and the C-S-H hydration products. However, such a procedure assumes that the slag peak shape does not change during hydration and thereby, the same reactivity for the individual SiO₄ species of the slag. Dyson *et al.* used a procedure for selective dissolution of the silicate species in the cement and its C-S-H hydration products, giving a residue which mainly includes the unreacted slag. A ²⁹Si MAS NMR spectrum of this residue, which was found to differ significantly from the spectrum of the anhydrous slag, was simulated and used as sub spectrum in the analysis of the spectrum for the hydrated Portland cement – slag mixture (3:1 w/w). The results indicated that a more reliable degree of slag hydration and quantification of the C-S-H hydrates can be obtained by this procedure [69].

Selective dissolution has also been utilized by Le Saout *et al.* [70] to characterize the spectral features in ²⁷Al MAS NMR spectra of the ferrite phase in class G oilwell cements, which generally contain high Fe₂O₃ contents. For the anhydrous cement with a C₄AF content of 14.4 wt.%, according to a Bogue calculation, the ferrite phase was isolated by dissolution of the calcium silicate and aluminates phases by salicylic acid – methanol and sugar – water solutions, respectively. The ²⁷Al MAS NMR spectrum (11.7 T, $\nu_R = 25$ kHz) of the isolated ferrite showed resonances from Al in tetrahedral and octahedral coordination with centers of gravity at

60 ppm and 6 ppm [70], in good agreement with an earlier reported ^{27}Al MAS NMR spectrum of a synthetic ferrite with the composition $\text{Ca}_2\text{Al}_{0.93}\text{Fe}_{0.17}\text{O}_5$ [71]. Furthermore, Le Saout *et al.* found that the severe loss of ^{27}Al NMR intensity, observed for the isolated ferrite phase as a result of strong dipolar couplings to the unpaired electrons of Fe^{3+} , indicates that Al present in the ferrite phase only gives a minor or negligible contribution to the ^{27}Al intensity in ^{27}Al MAS NMR spectra of oilwell cements, as proposed earlier from studies of synthetic calcium aluminoferrites [71]. However, reasonably well-resolved ^{29}Si MAS NMR spectra were obtained for the anhydrous and hydrated oilwell cement samples, allowing a determination of the degree of silicate hydration and the average silicate chain lengths for the C-S-H phases [70].

High-resolution ^1H , ^{17}O , and ^{29}Si MAS NMR have been widely used in the characterization of the basic structure of C-S-H phases. Improved information about modifications caused by variations in Ca/Si ratio has recently been gained from two-dimensional double-quantum homonuclear ^{29}Si - ^{29}Si correlation and ^1H - ^{29}Si heteronuclear chemical shift correlation MAS NMR experiments on synthetic C-S-H samples (Ca/Si = 0.7 – 1.5) enriched in ^{29}Si [72]. This is illustrated in Fig. 11 by the double-quantum ^{29}Si - ^{29}Si correlation MAS NMR experiment for a C-S-H with Ca/Si = 0.9. In the high-frequency region, Q^1 - Q^1 and Q^1 - Q^2 correlation peaks are observed, demonstrating the presence of dimeric units and Q^1 chain-end groups, respectively. The presence of a Q^3 resonance ($\delta(^{29}\text{Si}) = -92$ ppm) in the single-pulse ^{29}Si MAS NMR spectrum indicates the linking of two silicate chains in the interlayer space of the C-S-H, as found in the structure of 11-Å tobermorite. The ^{29}Si - ^{29}Si correlation experiment fully

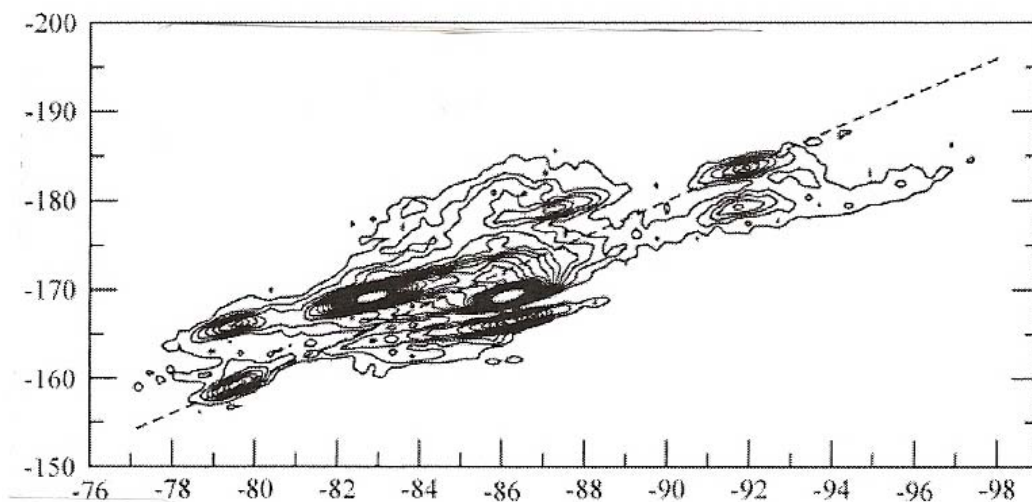


Fig. 11. ^{29}Si - ^{29}Si double-quantum correlation MAS NMR spectrum (11.7 T, $\nu_R = 10$ kHz) of a ^{29}Si enriched sample of C-S-H synthesized with Ca/Si = 0.9. The experiment is obtained by $^{29}\text{Si}\{^1\text{H}\}$ CP/MAS followed by the BAck to BAck (BABA) pulse sequence [73]. The vertical scale corresponds to the double-quantum dimension. Adapted from ref. [72].

supports this assignment by the observation of Q^3-Q^3 and Q^3-Q^{2v} peaks, where Q^{2v} denotes the SiO_4 tetrahedra adjacent to the Q^3 linking tetrahedra. Furthermore, the analysis of four C-S-H samples with Ca/Si ratios in the range 0.7 – 1.5 revealed a continuous decrease in silicate chain length with increasing Ca/Si ratio [72]. This agrees well with previous studies and a recent ^{29}Si MAS NMR investigation by Chen et al. [74] of two series of C-S-Hs with varying Ca/Si ratios, prepared from Ca_3SiO_5 hydration and the reaction of calcium nitrate with sodium silicate followed by decalcification by ammonium nitrate. ^{29}Si MAS NMR revealed that both preparations result in the above relationship between silicate chain length and Ca/Si ratio, however, with the chain lengths from the Ca_3SiO_5 preparation being consistently longer than those from the other synthetic procedure. This observation strongly suggests that the mean silicate chain length can vary in C-S-Hs with a given Ca/Si ratio [74]. Furthermore, these authors observed that the ^{29}Si chemical shifts for the Q^1 and Q^2 resonances slightly shift toward lower frequency with increasing Ca/Si ratio, an observation that may reflect minor changes in the C-S-H structure, although it cannot be immediately explained. The $^1H-^{29}Si$ heteronuclear chemical shift correlation CP/MAS experiments have shown correlation peaks for all Si sites and that water molecules are the main source of cross polarization for the C-S-H with low Ca content (Ca/Si = 0.7) [72]. For the C-S-H with a high Ca content (Ca/Si = 1.5), three 1H resonances can be resolved which have been assigned to H_2O , Ca-OH, and Si-OH protons. The two types of hydroxyl sites correlate with all Si sites of the C-S-H while correlations with the Q^1 , Q^{2P} , and Q^2 sites were observed for the water molecules.

The current status for ^{27}Al MAS NMR spectroscopy in studies of cementitious materials seems to be that the highest degree of resolution for resonances from different aluminate species is achieved by the single-pulse MAS experiment performed at high magnetic field ($B_0 \geq 14.1 - 21.1$ T), using high-power 1H decoupling and high-speed spinning ($\nu_R \geq 10$ kHz). This is primarily due to the high sensitivity for this spin nucleus, allowing studies of ^{27}Al in small concentrations, as well as the increased chemical shift dispersion and reduced second-order quadrupolar broadening with increased magnetic field strength. Thus, high magnetic fields of 17.5 T and 21.1 T have been utilized in studies of aluminium in synthetic C-S-H phases [75] and hydrated Portland cements [65,76], respectively. Illustrative examples from such analyses are shown in Fig. 12 by ^{27}Al MAS NMR spectra of a hydrated white Portland cement and a synthetic C-S-H sample prepared using the molar ratios Ca/Si = 1.00 and Al/Si = 0.05. The ^{27}Al MAS NMR spectrum of the hydrated Portland cement exhibits resonances from Al in 4-, 5-, and 6-fold coordination to oxygen atoms (Al[4], Al[5], and Al[6]) where a multiple-magnetic field investigation (7.1 – 21.1 T) of the Al[4] and Al[6] resonances has shown that these correspond to the ^{27}Al parameters $\delta_{iso} = 74.6$ ppm, $P_Q = C_Q(1 + \eta^2/3)^{1/2} =$

4.5 MHz and $\delta_{\text{iso}} = 39.9$ ppm, $P_Q = 5.1$ MHz, respectively [65]. The Al[4] peak is assigned to Al incorporated in bridging tetrahedra of dreierketten silicate chains of the C-S-H (Fig. 10) whereas there is significant evidence for that the penta-coordinated Al site is located in the interlayer of the C-S-H structure [75], potentially as Al^{3+} ions substituting for interlayer Ca^{2+} ions [76,77]. Of the three resonances originating from octahedrally coordinated Al, the high-frequency peaks at $\delta_{\text{iso}} = 13.1$ and 10.5 ppm are easily assigned to ettringite and monosulphate, respectively, or more correctly, AFt and AFm phases, since the anions in the columns of these structures only have a minor effect on the ^{27}Al NMR parameters for these phases.

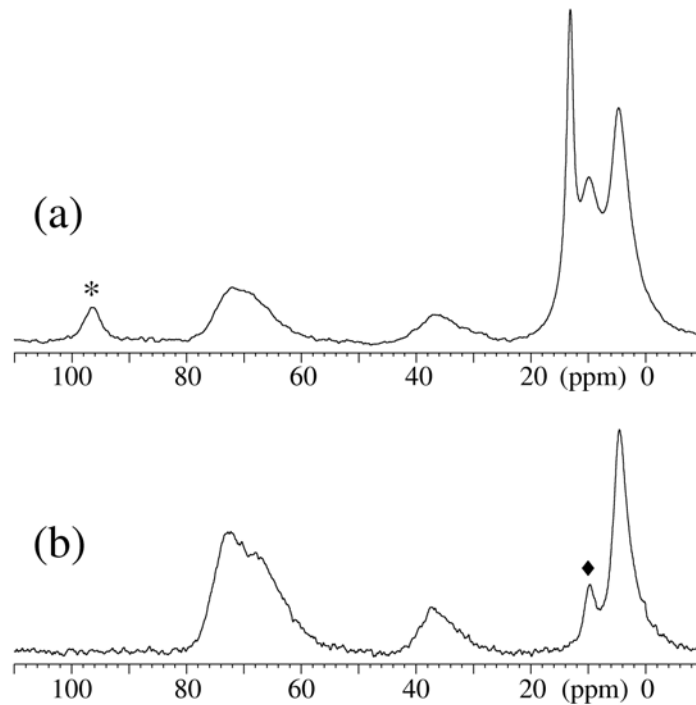


Fig. 12. ^{27}Al MAS NMR spectra (14.1 T, $\nu_R = 13.0$ kHz) of (a) a white Portland cement hydrated for 30 weeks and (b) a synthetic C-S-H sample synthesized with a Ca/Si ratio of 1.0. The asterisk denotes a spinning sideband from ettringite (AFt) and the diamond an impurity phase of $\text{CaO}\cdot\text{Al}_2\text{O}_3\cdot 10\text{H}_2\text{O}$ or an AFm phase.

The third Al[6] resonance, which corresponds to the parameters $\delta_{\text{iso}} = 5.0$ ppm and $P_Q = 1.2$ MHz, has been investigated in detail by Andersen *et al.* using a number of different NMR approaches [76]. For example, the observation of the resonance by $^{27}\text{Al}\{^1\text{H}\}$ CP/MAS NMR and its CP characteristics strongly suggest that it originates from $\text{Al}(\text{OH})_6^{3-}$ units while studies of heated samples shows that the resonance vanishes in samples heated above 70 – 90 °C. From the ^{27}Al MAS spectrum of the synthetic C-S-H (Fig. 12), it is apparent that the formation of this phase is associated with the C-S-H, in support of the final assignment of the third resonance to an amorphous/disordered aluminate hydroxide or a calcium

aluminate hydrate, produced either as a separate phase or as a nanostructured surface precipitate on the C-S-H phase [76]. The formation of an alumina-rich surface precipitate on the grain boundary of the C-S-H is in accord with observations by Taylor that the C-S-H and AFm phases are oppositely charged which may produce strong mutual attractions that can physically destroy the AFm crystals [78]. Thus, the constituent layers of the AFm may be dispersed in the C-S-H, resulting in a poorly crystalline phase which cannot be detected by XRD or thermal methods. In a ^{23}Na , ^{27}Al , and ^{29}Si MAS NMR study of the hydration products from granulated blast-furnace slag (gbfs) pastes activated by sodium hydroxide, sodium silicate, or calcium hydroxide, the third Al[6] resonance was only observed for gbfs samples activated by sodium silicate [79]. Employing arguments similar to those by Taylor [78], it was suggested that the resonance originates from an intimate mixture of C-S-H layers and AFm-like arrangements, potentially formed by intergrowth. Furthermore, it was proposed that the low-frequency shift of the 5-ppm resonance relative to $\delta(^{27}\text{Al})$ for pure AFm phases and the broadening of the Q^1 peaks in the ^{29}Si MAS NMR spectra for the silicate activated gbfs reflect that Al[6]–O–Si bonds are formed to Si sites of the C-S-H [79].

The incorporation of Al in the C-S-H structure has also been investigated in detail by Sun *et al.* [75] for a number of precipitated C-S-Hs exhibiting $\text{Ca}/(\text{Si} + \text{Al}) = 0.86 - 1.4$ and $\text{Al}/(\text{Al} + \text{Si}) = 0.0 - 0.3$. From high-field ^{27}Al MAS NMR spectra (17.5 T) they observed Al[4] peaks or shoulders with maxima at 58, 66, and 74 ppm. For different compositions of the C-S-Hs there were clear variations in the relative intensities but no changes in peak positions, indicating the presence of three different Al[4] species. This observation is also illustrated by the ^{27}Al MAS NMR spectrum of the C-S-H in Fig. 12 which clearly indicates the presence of two different Al[4] sites. Sun *et al.* assigned the three Al[4] resonances to Al in three types of bridging sites, a Q^3 bridging site across the interlayer ($\delta \approx 58$ ppm), a Q^2 site charge-balanced by interlayer Ca^{2+} , Na^+ or H^+ ions ($\delta \approx 66$ ppm), and a Q^2 site that is charge-balanced by interlayer or surface Al[5] and Al[6] sites through Al[4]–O–Al[5,6] linkages ($\delta \approx 74$ ppm) [75]. The latter assignment was based on the fact that XRD showed that the basal spacing of the tobermorite (C-S-H) samples increased significantly with increasing Al/(Al+Si) ratio [75]. Moreover, it is well-known from studies of other aluminosilicates that Al–O–Al bonds tend to shift the resonance towards higher frequency while Al–O–Si bonds result in a shift toward lower frequency. The observations by Sun *et al.* also indicated that Al does not enter the central Ca–O sheet or the pairing tetrahedra of the tobermorite-type layers and thus, they are compatible with the earlier mentioned observations on the structural mechanism for Al substitution into tobermorites and C-S-Hs [64–67,76].

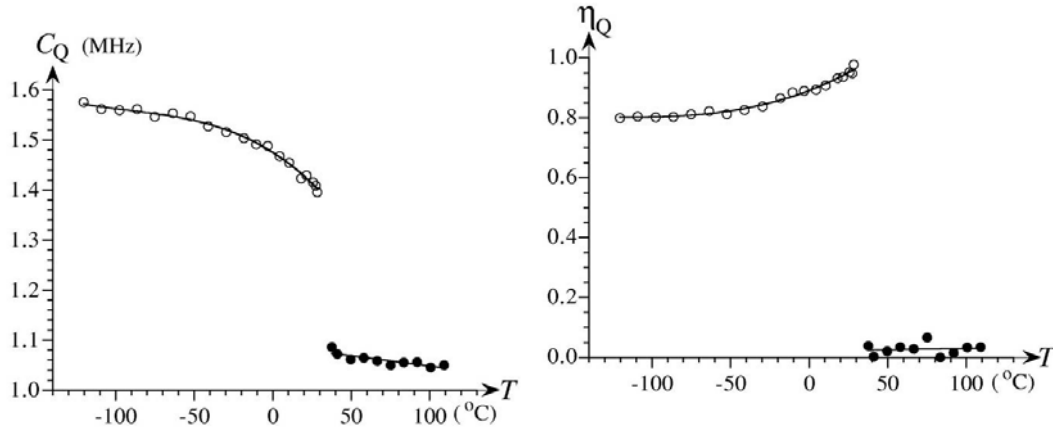


Fig. 13 Temperature dependence of the ^{27}Al quadrupole coupling parameters (C_Q and η_Q) for the low-temperature α -form (○) and high-temperature β -form (●) of Friedels salt. Adapted from ref. [80].

Variable-temperature ^{27}Al MAS NMR has been used to characterize the structural phase transition for Friedels salt ($\text{Ca}_2\text{Al}(\text{OH})_6\text{Cl}\cdot 2\text{H}_2\text{O}$) from the low-temperature monoclinic α -form to a rhombohedral β -form [80]. The abrupt change in ^{27}Al quadrupole coupling constants (C_Q) and associated asymmetry parameters (η_Q), determined from simulation of 29 ^{27}Al MAS NMR spectra in the range from -121 °C to 109 °C (Fig. 13), clearly reflect the phase transition around 34 °C. Moreover, an analysis of the corresponding ^{27}Al electric field gradients using simple model calculations reveals that hydrogen bonding plays an important role in the structural changes that occurs during the phase transition [80]. However, in contrast to C_Q and η_Q , the isotropic ^{27}Al chemical shift is almost independent of temperature with the value 9.2 ± 0.3 ppm at room temperature. This value and the actual data for C_Q and η_Q implies that centerband resonance for Friedels salt can hardly be resolved experimentally from the centerband from monosulphate (or other AFm phases, $\delta(^{27}\text{Al}) \approx 10.2$ ppm, $C_Q \approx 1.3 - 1.8$ MHz), as noted earlier [81], although this has been claimed in a recent ^{27}Al MAS NMR study of the aluminates hydrates in hardened Portland cements cured in chloride solutions [82]. However, from the Al_2O_3 and SO_3 mass balances derived from the ^{27}Al NMR intensities, assuming that SO_3 is present in ettringite and monosulphate only, an estimate of the upper and lower limits for the quantities of Friedels salt in hydrated cement pastes can be obtained [81]. Alternatively, Friedels salt may be detected by ^{35}Cl NMR, as justified by an earlier static-powder NMR study (11.7 T) of the phase transitions for a slightly carbonate-substituted sample of Friedels salt (e.g., $\text{Ca}_{1.96}\text{Al}_{1.04}(\text{OH})_6\text{Cl}_{0.76}(\text{CO}_3)_{0.14}\cdot 2.10\text{H}_2\text{O}$, phase transition at 6 °C) [83].

The influence of different organic admixtures on the hydration of Portland cement has been studied on the nanoscale by a number of different solid-state NMR methods by Rottstegge *et al.* [84,85]. For tile mortar systems

based on Portland cement, quartz, methyl cellulose, and different latex additives, $^{13}\text{C}\{^1\text{H}\}$ CP/MAS NMR showed that the poly(vinyl acetate co-ethylene) latex polymer was relatively stable towards hydrolysis in the alkaline medium of the hydrating Portland cement [84]. This was clearly seen by the absence of ^{13}C resonances from calcium acetate and poly(vinyl alcohol) which are formed in the cement matrix upon decomposition of the latex polymer. Furthermore, ^{29}Si MAS NMR revealed that the organic additives only have a minor influence on the silicate structure of the hardened cement whereas even small amounts of additives affects the calcium aluminate hydrates, i.e., the relative amounts of AFm and AFt phases, as revealed by ^{27}Al MAS NMR. For Portland cement (43.7 wt.%) – quartz (56.2 wt.%) mixtures, including 0.4 wt.% methyl cellulose or poly(vinyl alcohol co vinyl acetate) polymer, 2D double-quantum (BAck to BAck sequence [73]) and exchange (NOESY-type) MAS NMR experiments (with very high spinning speeds, $\nu_{\text{R}} = 30$ kHz) were used to detect connectivities between the organic additive and the inorganic components of the hardened cement material [85]. Weak double-quantum signals of the methyl cellulose with strongly bound H_2O molecules of the inorganic cement matrix were detected by ^1H double-quantum MAS NMR whereas the ^1H exchange experiment showed weak exchange signals of the poly(vinyl alcohol co vinyl acetate) polymer and the OH and H_2O species of the inorganic matrix. For both additives, this demonstrates a close proximity (~ 10 nm) of the organic admixture to the hydrated cement matrix which suggests that the additives are immobilized by adsorption onto the cement matrix or by incorporation into the hydrated cement paste [85].

5.2 ^1H relaxation NMR

The favorable NMR properties of ^1H along with its generally high abundance in cementitious materials make this spin nucleus the most sensitive NMR probe in studies of Portland cements. However, the small ^1H chemical shift range (~ 20 ppm) combined with significant line-broadening from strong homonuclear $^1\text{H} - ^1\text{H}$ dipolar interactions results in that high-resolution ^1H MAS NMR spectra is hard to obtain experimentally. However, the resolution increases with increasing magnetic field as well as spinning speed and very high-speed spinning MAS probes ($\nu_{\text{R}} > 30$ kHz) have recently become commercially available. On the other hand, supplementary information can be achieved from less technically demanding NMR experiments at low magnetic field that focus on spin-lattice (T_1) or spin-spin (T_2) relaxation times which can be rapidly measured by different pulse schemes, in some cases allowing a nearly continuous monitoring with time. For such *in situ* studies, the spin-spin relaxation time is particularly useful, since it is modulated by the motions of the species on which the spins reside and varies by several orders of

magnitude for ^1H of mobile or rigid water molecules and of hydroxyl groups. This variation allows extraction of different T_2 components along with the corresponding fraction of magnetization from multicomponent analysis of the intensities observed in free induction decays (FIDs) or spin-echo envelopes obtained by single-pulse or Carr-Purcell Meiboom-Gill (CPMG) pulse schemes, respectively. The approach has been utilized in recent ^1H T_2 studies of the hydrous species in hydrating white Portland cements [86,87]. From a non-linear least-squares analysis of the time-domain FIDs and CPMG decay curves, using a sum of exponential and Gaussian functions, a number of different magnetization components can be identified from the magnitude of the T_2 values as illustrated in Fig. 14. Generally, short T_2 values (10 – 20 μs) correspond to rigid ^1H sites as found in hydroxyl groups and water molecules in solids while long T_2 values reflect mobile water molecules in e.g. nano- or micro-sized pores. Following ^1H spin-spin relaxation studies of the hydration of C_3A [88] and C_3S model systems, Holly *et al.* identified five components with distinct T_2 values for a hydrating white Portland cement corresponding to (i) capillary pore water, (ii) solid-like crystalline water and OH^- groups (i.e., Portlandite, gypsum, and ettringite), (iii) mobile water molecules incorporated in the C-S-H phase, (iv) water molecules with restricted mobility in the C-S-H interlayer, and (v) secondary hydration water released by the decomposition of ettringite. The observation of the latter component, which constitutes only 3% of the total ^1H intensity, is quite unique. For the white Portland cement hydrated at room temperature ($w/c = 0.42$ [87]), the secondary hydration water is only present during the early hydration from 9 to 18 hours after which it is consumed by chemical reactions. In a similar

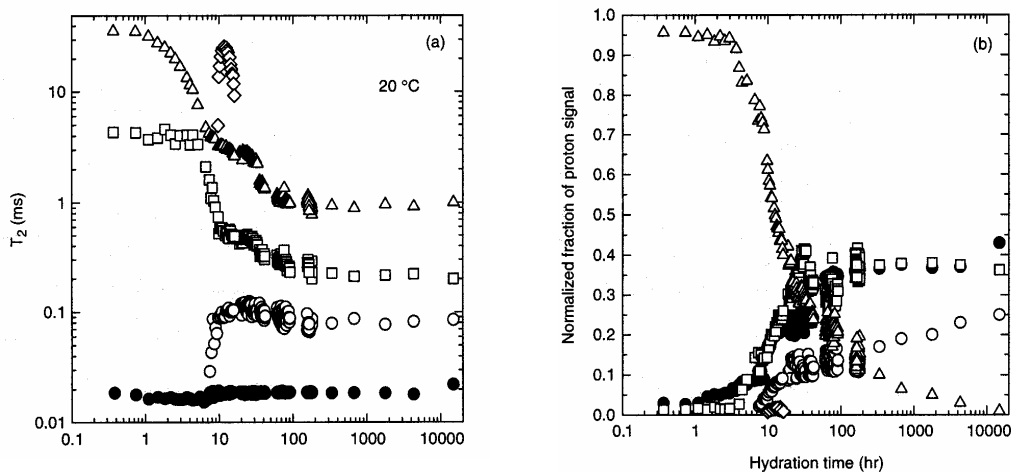


Fig. 14. ^1H T_2 values (left) and normalized magnetization fractions (right) as a function of the hydration time for a white Portland cement hydrated at 20 °C. The data are assigned to capillary pore water (triangles), mobile water in the C-S-H phase (squares), water molecules in the C-S-H interlayer (open circles), solid-like water and OH^- groups (filled circles), and secondary hydration water (diamonds). Adapted from ref. [87].

study of the CaO-Al₂O₃-SO₃-H₂O system [88], it was clearly observed that this component is associated with the water release following the formation of monosulphate at the expense of ettringite. Moreover, Holly *et al.* found that the secondary hydration water is present in the material at a significantly longer time in samples cured at elevated temperatures (60 and 100 °C) [87]. Similar T_2 spin-spin relaxation experiments, combined with MRI, has been used to study the hydration of white Portland cement in the presence of small amounts of organic waste materials (2-chloro-aniline) dissolved in methanol [89]. Three types of water molecules characterized by anisotropic (“solid-like” water), near isotropic (pore water), and isotropic (“free” water) motions were identified and the T_2 data for these species revealed a strong retardation of the hydration reactions in the presence of the organic additives, resulting in an significant extension of the dormant period [89].

The structural information that may be obtained from the spin-lattice relaxation time (T_1) has recently been analyzed in detail, in particular its dependency on paramagnetic ions and on the pore sizes confining the pore liquid. The relaxation model, which has been employed recently for the water-filled cement pores [90–92], is a biphasic fast exchange model [93] where the observed spin-lattice relaxation rate ($1/T_{1,obs}$) from water molecules in pores with a high surface-to-volume ratio, S/V , is governed by two contributions

$$\frac{1}{T_{1,obs}} = \frac{1}{T_{1,bulk}} + \frac{\varepsilon S}{V} \frac{1}{T_{1,surface}} \quad (3)$$

representing the bulk liquid ($T_{1,bulk}$) and water molecules on pore-surface sites ($T_{1,surface}$) where ε describes the thickness of the surface layer. For pores with a high S/V ratio, the dominating contribution to the relaxation rate comes from the hydrogens of the surface water molecules which reduces the analysis to an evaluation of $T_{1,surface}$ only. An expression for this term has been derived by Korb and coworkers [94,95], employing a model which assumes that temporarily adsorbed water molecules undergo a two-dimensional random walk on the pore surface and that the ^1H relaxation is primarily due to modulations of the dipole-dipole interactions between the ^1H spins and the electron spins of the paramagnetic impurities (e.g. Fe^{3+}) fixed on the surface. The diffusion of water molecules in the vicinity of fixed paramagnetic ions on the solid-liquid pore surface is characterized by a surface residence time, τ_s , and a translational correlation time, τ_m , associated with the individual molecular jumps of adsorbed molecules on the surface. This model may be applied to both the spin-spin ($1/T_{2,surface}$) and spin-lattice ($1/T_{1,surface}$) relaxation rates, and Korb *et al.* have showed that the ratio $T_{2,surface}/T_{1,surface}$ only depends on the NMR Larmor frequency and the τ_m , τ_s correlation times. From the expression for

this ratio and estimates of the two correlation times, it was subsequently predicted that the T_1 and T_2 values for water molecules in pores with high

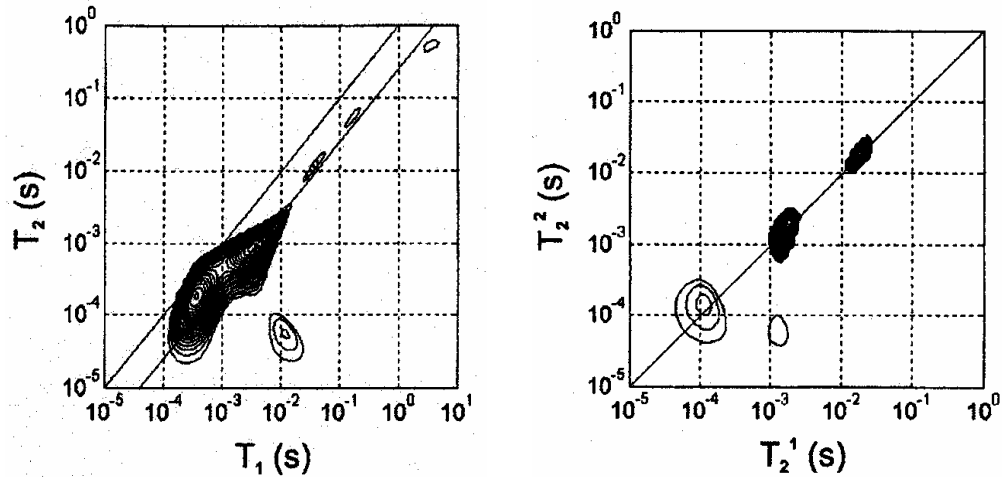


Fig. 15. ^1H T_1 - T_2 (left) and T_2 - T_2 correlation NMR spectra for a white Portland cement hydrated using a water to cement ratio of 0.4 and cured for 4 days at high humidity and 20 °C. The lower line in the T_1 - T_2 plot corresponds to the $T_1 = 4T_2$ line. The experiments were performed at a low Larmor frequency (20 MHz) employing an inversion-recovery followed by CPMG pulse sequence for the T_1 - T_2 spectrum and two CPMG sequences separated by a 10-ms delay for the T_2 - T_2 experiment. The spectra represent 2D inverse Laplace transformations of the experimental data. Adapted from ref. [91].

S/V ratios would fall in the range $T_1 = 2T_2 - 4T_2$ [91]. This relationship was utilized in a two-dimensional T_1 - T_2 correlation NMR experiment, employing the inversion-recovery pulse sequence to monitor T_1 followed by a CPMG sequence to detect the corresponding T_2 relaxation [91]. As an example, Fig. 15 illustrates the contour plot of such an experiment obtained by a 2D inverse Laplace transformation of the time-domain data for a white cement hydrated for 4 days. The correlation of T_1 and T_2 relaxation times in this spectrum shows five distinct peaks along the $T_1 = 4T_2$ line with a separation of approximately one order of magnitude between them. The peaks represent discrete pores with a pore size (i.e., S/V ratio) that increases for increasing relaxation times. Thus, the lowest peak, corresponding to $T_1 \approx 0.2$ ms, is assigned to gel pores with a dimension of a few nanometers whereas the remaining four peaks may reflect relaxation of water in capillary pores of increasing size [91]. The two peaks with lowest relaxation times ($T_1 \approx 0.2$ and 2 ms) and highest intensities exhibit a cross peak below the diagonal. This peak may be assigned to chemical exchange of water between the two different pores, i.e., water molecules that move between the pores on the timescale of the experiment, thereby indicating a transfer of water from capillary pores to gel pores. This interpretation is supported by the T_2 - T_2 correlation NMR spectrum of the same sample (Fig. 15) which also includes a small cross peak between the two peaks corresponding to lowest T_2 values [91]. The

T_2 - T_2 correlation spectrum is obtained by two CPMG sequences separated by a fixed delay of 10 ms in the actual case. This rather long delay suppresses water with short T_1 values which account for the reduced intensity of the $T_2 \approx 0.050$ ms peak and the increased intensity for the $T_2 \approx 20$ ms peak as compared to the intensities for those in the T_1 - T_2 correlation spectrum (Fig. 15a). The applicability of the T_1 - T_2 correlation experiment has been examined for the hydration (1 – 14 days) of a white Portland cement with and without added silica fume (10 wt%) [91]. The spectra showed a more continuous intensity distribution over the diagonal peaks in the silica fume samples, indicating that the silica fume disrupts the pore-size distribution of the developing larger pores. Furthermore, the reduced intensities of the off-diagonal peaks in the spectra of the silica fume pastes indicates that the chemical exchange of water between gel and capillary pore networks is reduced by silica fume [91]. McDonald *et al.* [92] have compared T_1 - T_2 correlation spectra following the early hydration (1 to 7 days) for two white Portland cements obtained from two different manufacturers. The distinct variations in these spectra, e.g. a continuous versus discrete pore-size distribution and the absence of off-diagonal peaks for one cement, originate from differences in microstructure for the two materials and were tentatively ascribed to reflect a difference in particle size for the two cements and potentially a degree of pre-hydration for one of the cements.

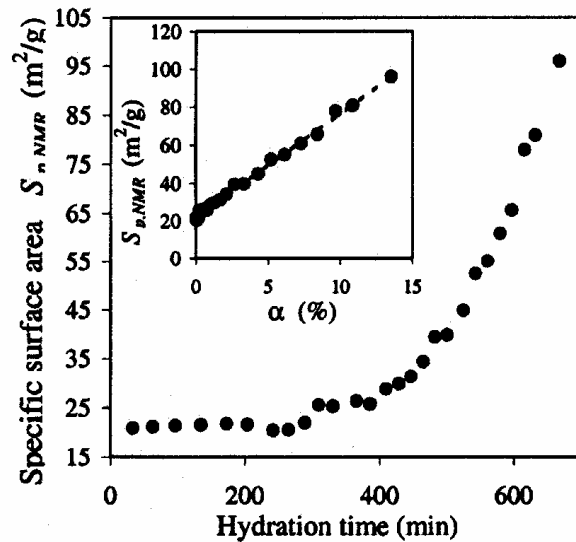


Fig. 16. Specific surface area (S_p) for a hydrating cement mortar (see text) as a function of hydration time, determined from analysis of ^1H T_1 relaxation rate field-cycling data. The inset illustrates S_p as a function of the degree of reaction (α) estimated from thermal analysis of the hydrating material. Adapted from ref. [96].

A clear separation of the T_1 relaxation associated with surface and bulk water (eq. (3)) confined within a hydrating cement can be obtained from nuclear magnetic relaxation dispersion (NMRD) experiments where the relaxation rate ($1/T_{1,obs}$) is measured as function of the Larmor frequency (ν_L), typically using field-cycling spectrometers where the magnetic field can be varied rapidly over the kHz – MHz range. From these experiments, specific features of the surface relaxation rate may be related to different processes of molecular surface dynamics. Barberon *et al.* have presented

a theoretical approach based on solid/liquid cross relaxation, proton surface diffusion, and nuclear paramagnetic relaxation that models the relaxation rates as a function of ν_L and from these data allow estimation of the specific surface area (S_p) for the material [96]. They demonstrated the method for a hydrating mortar (cement, sand, silica fume, water, superplasticizer, w/c = 0.38) by the analysis of relaxation rates measured for frequencies in the range 0.01 – 10 MHz. A field cycle in this frequency range took about 20 min and by progressive experiments, the hydration was followed for 12 hours. The specific surface areas, resulting from the NMRD analysis, as a function of hydration time (Fig. 16) reveal a nearly constant S_p value during the induction period while it increases rapidly after the time of setting. Moreover, a linear relationship is observed between S_p and the degree of reaction (α), estimated from thermal analysis [96], demonstrating that S_p is closely related to the nano-/micro-structural modifications that occur during hydration. A similar analysis of T_1 relaxation rates in field-cycling experiments has also been reported for a synthetic sample of tricalcium silicate hydrated for one year [97]. For this model sample, the ^1H relaxation exhibited a multi-exponential magnetization decay for each ν_L value. Thus, four relaxation-rate dispersion curves could be derived from these data and each fitted by the proposed relaxation model. With a preknowledge of the total amount of paramagnetic ions (Fe^{3+}) in the sample from an ESR spectrum [97], the model also allowed estimation of the average pore sizes, $\langle R_i \rangle = 1.8, 7.0, 50,$ and 600 nm, for the four classes of relaxation-rate dispersion curves. These average pore sizes are of the same magnitude as those estimated from T_1 – T_2 correlation NMR experiments.

^1H transverse relaxation approaches have also been used in dynamic studies of diffusion and moisture transport in hydrating cements. Generally, these methods, denoted NMR diffusometry, employ magnetic field gradients (constant or pulsed) synchronized with rf pulse schemes for spin-echo or stimulated spin-echo experiments to modify the decay of magnetization. The pulsed field gradients (PFGs) introduce an additional echo attenuation, resulting in an echo decay that is not a single-exponential. Theoretically, the decay of transverse magnetization can be expressed by two terms that describe the decay due to relaxation and diffusion, where analysis of the latter term provides a mean of extracting self-diffusion coefficients for the liquid phase in the material. The PFG NMR experiments are sensitive to molecular displacements in the μm range and seem particularly useful in studies of post-curing of cementitious materials [98] and of the diffusion of water into cement pastes [99]. The different approaches of field-gradient NMR in diffusion studies of hydrating cements have very recently been reviewed by Nestle *et al.* [100].

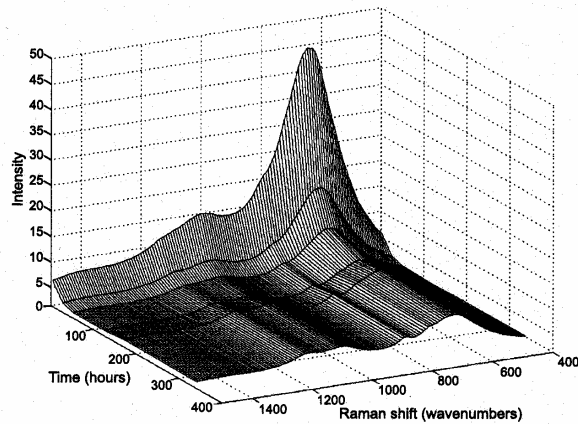
6. Raman spectroscopy

Infrared (IR) and Raman spectroscopies are often useful tools in the characterization of local structural features at the atomic level for solids since these techniques allow detection of amorphous as well as crystalline phases by measurement of vibrational frequencies that are sensitive to atomic masses and local symmetry. Of the two approaches, IR spectroscopy is the most well-established technique in cement chemistry and its ability to identify various anhydrous cement phases in a semi-quantitative manner is well documented [101]. Recently, there has been an increasing interest in applying Raman spectroscopy to cementitious systems and to explore the potential of this technique for these materials, although it is generally less sensitive than IR. However, Raman spectroscopy may benefit from the possibility of a range of instrumental configurations including a variety of different laser systems for excitation and filter units for spectral purification [102]. Moreover, the Raman microprobe instrument allows investigations on the μm -level from specific regions of a sample and it seems that this type of equipment is less sensitive to artifacts resulting from absorption and fluorescence [103].

Since the pioneering Raman study on cement minerals by Bensted [104], a number of investigations have reported Raman shifts for the different polymorphs of anhydrous calcium silicates, calcium aluminate and ferrite phases, observed either for synthetic samples or for these phases in Portland cements. A summary of these data can be found in recent reviews [102,105]. The cement minerals in their pure forms as well as in several commercial Portland cements have recently been critically examined by Fourier transform (FT) Raman spectroscopy by Newman *et al.* [106] using three different excitation frequencies (i.e., 1064, 632.8, and 514.5 nm). For pure samples of C_2S and C_3S as well as these phases in Portland cements they found that the bands in the Stokes region of the near infrared Raman spectra resulted primarily from fluorescence effects, since the corresponding bands in the anti-Stokes region were absent. Fluorescence phenomena depends on the excitation wavelength and thus, it can be judged whether a spectral band is a genuine Raman band or a fluorescence effect by measuring the Raman shifts using different excitation wavelengths. In this manner, Newman *et al.* identified true Raman shifts for C_3S and C_3A in Raman spectra recorded at two different visible light wavelengths and found these to be in good agreement with earlier reported data [107]. Furthermore, Newman *et al.* [106] found that the fluorescence in the near-infrared Raman spectra are strongly dependent on trace amounts of transition metal impurities and that the fluorescence effects vary significantly for different Portland cements. However, the intensities of the different fluorescence peaks, observed by in-situ near-infrared Raman spectra for different Portland cement pastes, were found to progressively decrease with the hydration time as illustrated

in Fig. 17. The most significant changes in the spectra occurred between 3 and 48 hours, indicating that the in-situ measurement of the decrease in fluorescence represents a new method for monitoring cement hydration. Newman *et al.* tentatively assigned the strong fluorescence from the calcium silicate minerals and Portland cements to the fact that these samples include orthosilicates as the dominating component, since a significantly lower degree of fluorescence was observed for a metasilicate (wollastonite) sample [106]. Thus, they proposed that the fluorescence is associated with the presence of isolated SiO_4 tetrahedra which may also explain the decrease in intensity in the in-situ experiments as the hydration proceeds and linked SiO_4 tetrahedra are formed.

Fig. 17. In-situ near-infrared FT Raman spectra following the hydration of a Portland cement paste. The Raman shifts are relative to the laser (1064 nm). Adapted from ref. [106].

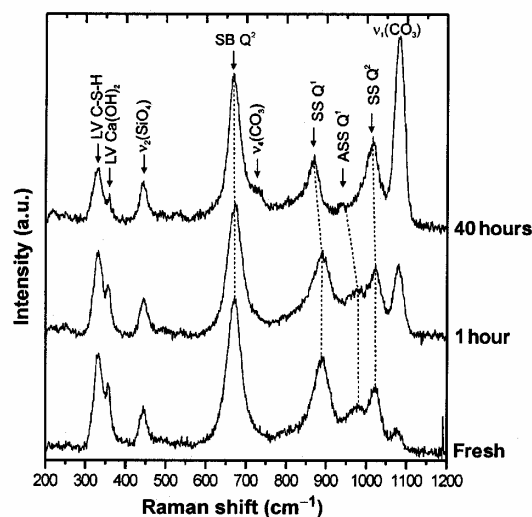


Raman spectroscopy has been increasingly used in studies of carbonation reactions in cementitious materials, utilizing the $\nu_1[\text{CO}_3^{2-}]$ band at 1085 cm^{-1} with a high scattering cross-section. The three polymorphs of CaCO_3 , i.e. calcite, aragonite, and vaterite, can be distinguished from their Raman spectra as employed in a recent micro-Raman study of the CaCO_3 polymorphs formed at different depths in a carbonated lime mortar as a result of CO_2 diffusion [108]. For the less thermodynamically stable form, vaterite, Raman spectroscopy has been used to identify the specific symmetry of the carbonate anion in this form [109] which gave a result that was only compatible with one of the three different crystal structures proposed for vaterite, i.e. the hexagonal structure with carbonate anions in a C_s site of the $P6_3/mmc$ space group. Furthermore, three different CaCO_3 hydrates, $\text{CaCO}_3 \cdot \text{H}_2\text{O}$, $\text{CaCO}_3 \cdot 6\text{H}_2\text{O}$, and an amorphous CaCO_3 hydrate, have been characterized by Raman spectroscopy [110]. These hydrates are considered as precursors for the anhydrous CaCO_3 polymorphs and valuable insight into the transformation mechanisms have been derived from *in-situ* Raman studies of the dehydration of these hydrates at different temperatures.

The type and extent of carbonation for synthetic C-S-H phases, the so-called C-S-H(I)'s, prepared with synthesis Ca/Si ratios ranging from 0.2 to 1.5 and exposed to air for up to 6 months have been investigated by

Raman spectroscopy [111,112]. Although the samples were handled under nitrogen during the mechano-chemical preparation and prior to the Raman measurements, the Raman spectra of the fresh samples show a weak $\nu_1[\text{CO}_3^{2-}]$ band at 1080 cm^{-1} , indicating that surface carbonation starts immediately upon exposure to air [111]. The detection of carbonate ions is illustrated in Fig. 18 by Raman spectra following the early carbonation for the C-S-H(I) with $\text{Ca/Si} = 1.50$. Although, the level of carbonation is low in these samples, it is apparent that the amount of calcium carbonate increases significantly by prolonged exposure to air, as manifested by the increase in intensity for the $\nu_1[\text{CO}_3^{2-}]$ band at 1080 cm^{-1} and by the observation of the $\nu_4[\text{CO}_3^{2-}]$ band at 725 cm^{-1} after 40 hours. From the relative large line width of the $\nu_1[\text{CO}_3^{2-}]$ band, Black *et al.* [112] concluded that this band originates from amorphous calcium carbonate hydrate, since the corresponding bands from the crystalline CaCO_3 polymorphs are much narrower. Furthermore, they found that the calcium carbonate hydrate is formed by consumption of portlandite, present as an additional phase in the samples, or by decalcification of the C-S-H(I) phase as seen by an increased silicate polymerization. The presence of portlandite results in a significant increase in carbonation and its consumption is apparent from the decrease in intensity of the Ca–O lattice vibration (LV) at 359 cm^{-1} (Fig. 18). From studies of the C-S-H(I) samples on a longer time scale, Black *et al.* observed that the amorphous calcium carbonate hydrate was always the initial carbonation product. With time this phase crystallized either as predominantly vaterite (for $\text{Ca/Si} \geq 0.67$) or aragonite ($\text{Ca/Si} \leq 0.5$), however, calcite was not detected in any of the samples.

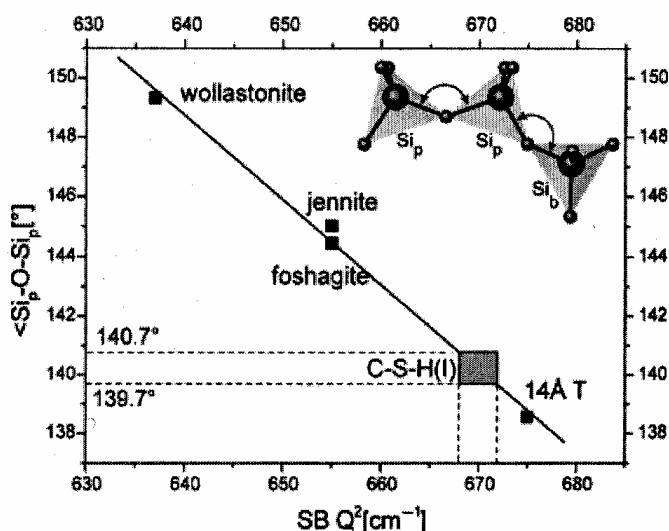
Fig. 18. Raman spectra of a C-S-H(I) synthesized with $\text{Ca/Si} = 1.50$ and handled under nitrogen prior to the Raman experiment. The spectra correspond to this sample exposed to air during the experiment (“fresh”) and for 1 and 40 hours. Adapted from ref. [112].



The fresh C-S-H(I) samples prior to carbonation were investigated in closed capillaries in detail by Raman spectroscopy by Garbev *et al.* [111] and the frequencies, line widths, and intensities of the internal vibrations of the silicate anions, the Ca-O lattice vibrations, and the OH stretching

bands were evaluated in terms of the Ca/Si ratios used in the synthesis. For the silicate network, sharp Q^2 and Q^1 bands were observed for samples with low Ca/Si ratios, indicating the presence of uniformly distributed long chains and end groups of SiO_4 tetrahedra, respectively, whereas the depolymerization of the silicate chains with increasing Ca/Si ratio resulted in a broadening of the bands and a shift of the Q^2 symmetrical stretching from 1010 cm^{-1} to 1022 cm^{-1} . Furthermore, for the C-S-H(I)'s prepared with increasing Ca/Si ratio from 0.5 to 1.5, the Si-O-Si symmetrical bending band shifted slightly from 668 cm^{-1} to 672 cm^{-1} . This band was assigned to the bending for two paired SiO_4 tetrahedra (i.e. Si_p-O-Si_p) and a comparison of these frequencies with the linear relationship observed between the Si_p-O-Si_p bending bands and the average Si_p-O-Si_p bond angle for some crystalline calcium silicates (Fig. 19) strongly suggest that the mean Si_p-O-Si_p bond angles in the C-S-H(I)'s were in the range $139.7 - 140.7^\circ$. Thus, the silicate network of the C-S-H(I)'s exhibits an average paired bond angle that is very close to 140° which is the energetically favored bond angle in silicate minerals [111].

Fig. 19. Average Si_p-O-Si_p bond angles obtained from X-ray structural data as a function of the Si_p-O-Si_p symmetrical bending (SB) frequencies in Raman spectra for the calcium silicates, wollastonite, jennite, foshagite, and 14-Å tobermorite. Adapted from ref. [111].



Raman spectroscopy has also been used to follow the water vapour hydration (one week to 6 months) of an oil-well cement in the presence of carbon dioxide [113]. After one week, Raman bands from portlandite and ettringite were observed while the silicate bands indicated that these early hydration products were formed on the alite grains. Furthermore, it was found that carbon dioxide participates in the surface reactions by forming calcium carbonate via reaction with portlandite. Finally, micro-Raman spectroscopy has proven useful for identification of thaumasite in field concrete samples [114,115] using the characteristic Raman bands at 688 , 990 , and 1072 cm^{-1} from octahedrally coordinated Si, sulphate and carbonate anions, respectively, which in combination allow differentiation of thaumasite from ettringite, gypsum, and calcium carbonate.

7. Conclusions and comments

What is the ultimate characterisation? Perhaps the ultimate goal of cement chemistry is to describe where every atom starts, where each ends up and how and why they get there. The aim is therefore a comprehensive transformation pathway. In this light, then characterization methods must provide chemical and structural information at all appropriate scales and throughout transformation process.

Perhaps it is then clear that two things are missing. First, the solution phase remains something of a terra incognita. We simply do not have methods today which can tell us what the solution composition is either on the bulk or the microscale. Since many of the transformations (perhaps almost all) involve ions passing through solution, this is a most serious lack.

Second, we require further methods of distinguishing between surface and bulk materials. Cements are compositionally heterogeneous on many length scales; the anhydrous materials have the further complication of a large asymmetric particle size distribution and the hydrated materials a complex porosity. At present the chemical characterization methods almost entirely ignore such matters. In a future Congress, we hear a different story.

8. References

- [1] G.E. Pake. Nuclear resonance absorption in hydrated crystals: fine structure of the proton line. *Journal of Chemical Physics* 16 (1948) 327 – 36.
- [2] M.R. Hartman, S.K. Brady, R. Berliner, M.S. Conrad. The evolution of structural changes in ettringite during thermal decomposition. *Journal of Solid State Chemistry* 179 (2006) 1259 – 1272.
- [3] J.C. Taylor, I. Hinczak, C.E. Matulis. Rietveld full-profile quantification of Portland cement clinker: The importance of including a full crystallography of the major phase polymorphs. *Powder Diffraction* 15 (2000) 7 – 18.
- [4] V. Peterson, B. Hunter, A. Ray, L.P. Aldridge. Rietveld refinement of neutron, synchrotron and combined powder diffraction data of cement clinker. *Applied Physics A, Suppl* 74 (2002) S1409 – S1411.

- [5] V.K. Peterson. Diffraction Investigations of Cement Clinker and Tricalcium Silicate using Rietveld Analysis. PhD thesis, University of Technology, Sydney 2003. <http://hdl.handle.net/2100/328>
- [6] V.K. Peterson, B. A. Hunter, A.S. Ray. A comparative study of Rietveld phase analysis of cement clinker using neutron, laboratory X-ray, and synchrotron data. *Powder Diffraction* 21 (2006) 12 – 18.
- [7] O. Pritula, L. Smrcok, B. Baumgartner, On reproducibility of Rietveld analysis of reference Portland cement clinkers. *Powder Diffraction* 18 (2003) 16–22.
- [8] O. Pritula, L. Smrcok, J. Ivan and K. Izdinsky. X-ray quantitative phase analysis of residues of the Reference Portland clinkers. *Ceramics–Silikaty* 48 (2004) 34 – 39.
- [9] O. Pritula, L. Smrcok, D.M. Többens, V. Langer. X-ray and neutron Rietveld quantitative phase analysis of industrial Portland cement clinkers. *Powder Diffraction* 19 (2004) 232 – 239.
- [10] N.V.Y. Scarlett, I.C. Madsen, C. Manias, D. Retallack. On-line X-ray diffraction for quantitative phase analysis: Application in the Portland cement industry. *Powder Diffraction* 16 (2001) 71 – 80.
- [11] P. Stutzman. Powder diffraction analysis of hydraulic cements: ASTM Rietveld round-robin results on precision. *Powder Diffraction* 20 (2005) 97 – 100.
- [12] A.G. de la Torre, A. Cabeza, A. Calvente, S. Bruque, and M.A.G. Aranda. Full phase analysis of Portland clinker by penetrating synchrotron powder diffraction. *Analytical Chemistry* 73 (2001) 151 – 156.
- [13] A.G. De la Torre, M.A.G. Aranda. Accuracy in Rietveld quantitative phase analysis of Portland cements. *Journal of Applied Crystallography* 36 (2003) 1169 – 1176.
- [14] A.G. de la Torre, E.R. Losilla, A. Cabeza and M.A.G. Aranda. High-resolution synchrotron powder diffraction analysis of ordinary Portland cements: Phase coexistence of alite. *Nuclear Instruments and Methods in Physics B* 238 (2005) 87 – 91.
- [15] A.G. de la Torre, A. Cabeza, E.R. Losilla and M.A.G. Aranda. Quantitative phase analysis of ordinary Portland cements using synchrotron radiation powder diffraction. *Zeitschrift für Kristallographie Suppl* 23 (2006) 587 – 592.

- [16] G. Walenta, T. Füllmann. Advances in quantitative XRD analysis for clinker, cements, and cementitious additions. *Powder Diffraction* 19 (2004) 40 – 44.
- [17] G. Walenta, T. Füllmann. Advances in quantitative XRD analysis for clinker, cements, and cementitious additions. *Advances in X-ray Analysis* 47 (2004) 287 – 296.
- [18] A. Crumbie, G. Walenta, T. Füllmann. Where is the iron? Clinker microanalysis with XRD Rietveld, optical microscopy/point cutting, Bogue and SEM – EDS techniques. *Cement and Concrete Research* 36 (2006) 1542 – 1547.
- [19] M.-N. de Noirfontaine, F. Dunstetter, M. Courtial, G. Gasecki, M. Signes-Frehel. Polymorphism of tricalcium silicate, the major compound of cement clinker. 2. Modelling alite for Rietveld analysis, an industrial challenge. *Cement and Concrete Research* 36 (2006) 54 – 64.
- [20] V.K. Peterson. A Rietveld refinement investigation of a Mg-stabilized triclinic tricalcium silicate using synchrotron X-ray powder diffraction data. *Powder Diffraction* 19 (2004) 356 – 358.
- [21] V.K. Peterson, B.A. Hunter, A. Ray. Tricalcium silicate T_1 and T_2 polymorphic investigations: Rietveld refinement at various temperatures using synchrotron powder diffraction. *Journal of the American Ceramic Society* 87 (2004) 1625 – 1634.
- [22] D. Stephan, S. Wistuba. Crystal structure refinement and hydration behaviour of $3\text{CaO}\cdot\text{SiO}_2$ solid solutions with MgO , Al_2O_3 and Fe_2O_3 . *Journal of the European Ceramic Society* 26 (2006) 141 – 148.
- [23] K. Mori, R. Kiyonagi, M. Yonemura, K. Iwase, T. Sato, K. Itoh, M. Sugiyama, T. Kamiyama, T. Fukunaga. Charge state of Ca atoms in β -dicalcium silicate. *Journal of Solid State Chemistry* 179 (2006) 3286 – 3294.
- [24] K.L. Scrivener, T. Füllmann, E. Gallucci, G. Walenta, E. Bermejo. Quantitative study of Portland cement hydration by X-ray diffraction/Rietveld analysis and independent methods. *Cement and Concrete Research* 34 (2004) 1541 – 1547.
- [25] J.M. Rivas Mercury, X. Turrillas, A.H. de Aza, P. Pena. Calcium aluminates hydration in presence of amorphous SiO_2 . *Journal of Solid State Chemistry* 179 (2006) 2988 – 2997.
- [26] N. Meller, C. Hall, K. Kyritsis, G. Giritat. Synthesis of cement based $\text{CaO}\text{--}\text{Al}_2\text{O}_3\text{--}\text{SiO}_2\text{--}\text{H}_2\text{O}$ (CASH) hydroceramics at 200 and 250 °C: Ex-situ

and in-situ diffraction. *Cement and Concrete Research* 37 (2007) (in press)

[27] A.N. Christensen, T.R. Jenson, N.V.Y. Scarlett, I.C. Madsen, J.C. Hanson. Hydrolysis of pure and sodium substituted calcium aluminates and cement clinker components investigated by *in situ* synchrotron X-ray powder diffraction. *Journal of the American Ceramic Society* 87 (2004) 1488 – 1493.

[28] H.F.W. Taylor. Modification of the Bogue calculation. *Advances in Cement Research* 2 (1989) 73 – 77.

[29] C. Hall and K. L. Scrivener. Oilwell cement clinkers: X-ray micro-analysis and phase composition. *Advanced Cement Based Materials* 7 (1998) 28 - 38.

[30] T.L. Hughes, Schlumberger Cambridge Research, Cambridge, UK (unpublished data).

[31] L.D. Mitchell, P.S. Whitfield and J.J. Beaudoin. The effects of particle statistics on quantitative Rietveld analysis of cement. *International Congress on the Chemistry of Cement, Montreal (2007)*: in press

[32] G.J. Redhammer, G. Tippelt, G. Roth, G. Amthauer, Structural variations in the brownmillerite series $\text{Ca}_2(\text{Fe}_{2-x}\text{Al}_x)\text{O}_5$: Single-crystal X-ray diffraction at 25 °C and high-temperature X-ray powder diffraction ($25\text{ °C} \leq T \leq 1000\text{ °C}$). *American Mineralogist* 89 (2004) 405 – 420.

[33] M. Zöttl and H. Pöllmann. Stability and properties of brownmillerites $\text{Ca}_2(\text{Al},\text{Mn},\text{Fe})_2\text{O}_5$ and perovskites $\text{Ca}(\text{Mn},\text{Fe})\text{O}_{3-x}$ in the system $\text{Ca}_2\text{Fe}_2\text{O}_5$ – “ $\text{Ca}_2\text{Mn}_2\text{O}_5$ ” – “ $\text{Ca}_2\text{Al}_2\text{O}_5$ ”. *Journal of the American Ceramic Society* 89 (2006) 3491 – 3497.

[34] A.C. Jupe, J.K. Cockcroft, P. Barnes, S.L. Colston, G. Sankar, C. Hall. The site occupation of Mg in the brownmillerite structure and its effect on hydration properties. *Journal of Applied Crystallography* 34 (2001) 55–61.

[35] I.G. Richardson, C. Hall, G.W. Groves. The composition and structure of the interstitial phase in an oilwell cement clinker. *Advances in Cement Research* 5 (1993) 15 – 21.

[36] A. Gloter, J. Ingrin, D. Bouchet, K. Scrivener, C. Colliex. TEM evidence of perovskite-brownmillerite coexistence in the $\text{Ca}(\text{Al}_x\text{Fe}_{1-x})\text{O}_{2.5}$ system with minor amounts of titanium and silicon. *Physics and Chemistry of Minerals* 27 (2000) 504 – 513.

- [37] E. Bonaccorsi, S. Merlino, A.R. Kampf. The crystal structure of tobermorite 14 Å (plombierite), a C-S-H phase. *Journal of the American Ceramic Society* 88 (2005) 505 – 512.
- [38] E. Bonaccorsi, S. Merlino, H.F.W. Taylor. The crystal structure of jennite, $\text{Ca}_9\text{Si}_6\text{O}_{18}(\text{OH})_6 \cdot 8\text{H}_2\text{O}$. *Cement and Concrete Research* 34 (2004) 1481 – 1488.
- [39] S. Merlino, E. Bonaccorsi, T. Armbruster. The real structure of tobermorite 11 angstrom: normal and anomalous forms, OD character and polytypic modifications. *European Journal of Mineralogy* 13 (2001) 577 – 590.
- [40] C. Hejny, T. Armbruster. Polytypism in xonotlite $\text{Ca}_6\text{Si}_6\text{O}_{17}(\text{OH})_2$. *Zeitschrift für Kristallographie* 216 (2001) 396 – 408.
- [41] A.G. De la Torre, M.-G. López-Olmo, C. Álvarez-Rua, S. García-Granda, M.A.G. Aranda. Structure and microstructure of gypsum and its relevance to Rietveld quantitative phase analyses. *Powder Diffraction* 19 (2004) 240 – 246.
- [42] K. Garbev. Structure, properties and quantitative Rietveld analysis of calcium silicate hydrates (C-S-H phases). PhD thesis, Ruprecht-Karls-University, Heidelberg 2004.
- [43] M.R. Hartman, R. Berliner. Investigation of the structure of ettringite by time-of-flight neutron powder diffraction techniques. *Cement and Concrete Research* 36 (2006) 364 – 370.
- [44] F. Goetz-Neunhoeffler, J. Neubauer. Refined ettringite ($\text{Ca}_6\text{Al}_2(\text{SO}_4)_3 \cdot (\text{OH})_{12} \cdot 26\text{H}_2\text{O}$) structure for quantitative X-ray diffraction analysis. *Powder Diffraction* 21 (2006) 4 – 11.
- [45] A.E. Moore, H.F.W. Taylor. Crystal structure of ettringite. *Acta Crystallographica B: Structural Crystallography* 26 (1970) 386 – 393.
- [46] Q. Zhou, E.E. Lachowski, F.P. Glasser, Metaettringite, a decomposition product of ettringite, *Cement and Concrete Research* 34 (2004) 703 – 710.
- [47] N. Greaves and Å. Kvik. Synchrotron radiation in materials science. *Nuclear Instruments and Methods in Physics Research B* 238 (2005) 1 – 4.
- [48] P. Barnes, S. L. Colston, A. C. Jupe, S. D. M. Jacques, M. Attfield, R. Pisula, S. Morgan, C. Hall, P. Livesey, S. Lunt, The use of synchrotron sources in the study of cement materials. In: J. Bensted and P. Barnes

(Eds.), *Structure and Performance of Cements*, Second edn, Spon Press, London & New York, 2002, pp. 477 – 499.

[49] T.R. Jensen, A.N. Christensen, J.C. Hansen. Hydrothermal transformation of the calcium aluminum oxide hydrates $\text{CaAl}_2\text{O}_4 \cdot 10\text{H}_2\text{O}$ and $\text{Ca}_2\text{Al}_2\text{O}_5 \cdot 8\text{H}_2\text{O}$ to $\text{Ca}_3\text{Al}_2(\text{OH})_{12}$ investigated by in situ synchrotron X-ray powder diffraction. *Cement and Concrete Research* 35 (2005) 2300 – 2309.

[50] R.J. Cernik, P. Barnes, G. Bushnell-Wye, A.J. Dent, G.P. Diakun, J.V. Flaherty, G.N. Greaves, E.L. Heeley, W. Helsby, S.D.M. Jacques, J. Kay, T. Rayment, A. Ryan, C.C. Tanga, N.J. Terrill. The new materials processing beamline at the SRS Daresbury, MPW6.2. *Journal of Synchrotron Radiation* 11 (2004) 163 – 170.

[51] L. Tunna, P. Barclay, R.J. Cernik, K.H. Khor, W. O'Neill, P. Seller. The manufacture of a very rapid high precision X-ray collimator array for rapid tomographic energy-dispersive diffraction imaging. *Measurement Science and Technology* 17 (2006) 1767 – 1775.

[52] A. Steuwer, J.R. Santisteban, M. Turski, P.J. Withers, T. Buslaps. High-resolution strain mapping in bulk samples using full-profile analysis of energy-dispersive synchrotron X-ray diffraction data, *Journal of Applied Crystallography* 37 (2004) 883 – 889.

[53] J.J. Biernacki, C.J. Parnham, T.R. Watkins, C.R. Hubbard, J. Bai. Phase-resolved strain measurements in hydrated ordinary Portland cement using synchrotron X-rays. *Journal of the American Ceramic Society* 89 (2006) 2853 – 2859.

[54] B. Benedikt, M. Lewis, P. Rangaswamy. Measurement and modeling of internal stresses at microscopic and mesoscopic levels using micro-Raman spectroscopy and X-ray diffraction. *Powder Diffraction* 21 (2006) 118 – 121.

[55] N. Meller, University of Edinburgh, Edinburgh, UK, (unpublished results).

[56] A.M. Scheidegger, M. Vespa, D. Grolimund, E. Wieland, M. Harfouche, I. Bonhoure, R. Dähn, The use of (micro)-X-ray absorption spectroscopy in cement research, *Waste Management* 26 (2006) 699 – 705.

[57] M. Vespa, R. Daehn, E. Gallucci, D. Grolimund, E. Wieland, A.M. Scheidegger. Microscale investigations of Ni uptake in cement using a combination of scanning electron microscopy and synchrotron-based

techniques. *Environmental Science and Technology* 40, (2006) 7702 – 7709.

[58] J. Rose, A. Bénard, S. El Mrabet, A. Masion, I. Moulin, V. Briois, L. Olvi, J.-Y. Bottero, Evolution of iron speciation during hydration of C₄AF, *Waste Management* 26 (2006) 720 – 724.

[59] A.M. Beale, A.M.J. van der Eerden, S.D.M. Jacques, O. Leynaud, M.G. O'Brien, F. Meneau, S. Nikitenko, W. Bras, B.M. Weckhuysen. A combined SAXS/WAXS/XAFS setup capable of observing concurrent changes across the nano-to-micrometer size range in inorganic solid crystallization processes. *Journal of the American Chemical Society* 128 (2006) 12386 – 12387.

[60] P. Colombet and A.-R. Grimmer (Eds.), *Application of NMR spectroscopy to cement science*, Gordon & Breach Science, Amsterdam, 1994.

[61] P. Colombet, A.-R- Grimmer, H. Zanni, P. Sozzani (Eds.), *Nuclear magnetic Resonance Spectroscopy of Cement-Based Materials*, Springer-Verlag, Berlin, 1998.

[62] J. Skibsted, C. Hall, H.J. Jakobsen, Nuclear magnetic resonance spectroscopy and magnetic resonance imaging of cements and cement-based materials, in: J. Bensted and P. Barnes (Eds.), *Structure and Performance of Cements*, Second edn, Spon Press, London & New York, 2002, pp. 457 – 476.

[63] H. Krøyer, H. Lindgreen, H.J. Jakobsen, J. Skibsted, Hydration of Portland cement in the presence of clay minerals studied by ²⁹Si and ²⁷Al MAS NMR spectroscopy, *Advances in Cement Research* 15 (2003) 103 – 112.

[64] I.G. Richardson, A.R. Brough, R. Brydson, G.W. Groves, C.M. Dobson, Location of aluminium in substituted calcium silicate hydrate (C-S-H) gels as determined by ²⁹Si and ²⁷Al NMR and EELS, *Journal of the American Ceramic Society* 76 (1993) 2285 – 2288.

[65] M. D. Andersen, H.J. Jakobsen, J. Skibsted, Incorporation of aluminum in the calcium silicate hydrate (C-S-H) phase of hydrated Portland cements: A high-field ²⁷Al and ²⁹Si MAS NMR study, *Inorganic Chemistry* 42 (2003) 2280 – 2287.

- [66] I.G. Richardson, G.W. Groves, The structure of the calcium silicate hydrate phases present in hardened paste of white Portland cement/blast-furnace slag blends, *Journal of Materials Science* 32 (1997) 4793 – 4802.
- [67] M.D. Andersen, H.J. Jakobsen, J. Skibsted, Characterization of white Portland cement hydration and the C-S-H structure in the presence of sodium aluminate by ^{27}Al and ^{29}Si MAS NMR spectroscopy, *Cement and Concrete Research* 34 (2004) 857 – 868.
- [68] C.A. Love, I.G. Richardson, A.R. Brough, Composition and structure of C-S-H in white Portland cement – 20% metakaolin pastes hydrated at 25 °C, *Cement and Concrete Research* 37 (2007) 109 – 117.
- [69] H.M. Dyson, I.G. Richardson, A.R. Brough, A combined ^{29}Si MAS NMR and selective dissolution technique for the quantitative evaluation of hydrated blast furnace slag cement blends, *Journal of American Ceramic Society* 90 (2007) 598 – 602.
- [70] G. Le Saout, E. Lécotier, A. Rivereau, H. Zanni, Chemical structure of cement aged at normal and elevated temperatures and pressures: Part I. Class G oilwell cement, *Cement and Concrete Research* 36 (2006) 71 – 78.
- [71] J. Skibsted, H.J. Jakobsen, C. Hall, Quantitative aspects of ^{27}Al MAS NMR of calcium aluminoferrites, *Advanced Cement Based Materials* 7 (1998) 57 – 59.
- [72] F. Brunet, P. Bertani, T. Charpentier, A. Nonat, J. Virlet, Application of ^{29}Si homonuclear i heteronuclear NMR correlation to structural studies of calcium silicate hydrates, *Journal of Physical Chemistry B* 108 (2004) 15494 – 15502.
- [73] M. Feike, D.E. Demco, R. Graf, J. Gottwald, S. Hafner, H.W. Spiess, Broadband multiple-quantum NMR spectroscopy, *Journal of Magnetic Resonance A*, 122 (1996) 214 – 221.
- [74] J.J. Chen, J.J. Thomas, H.F.W. Taylor, H.M. Jennings, Solubility and structure of calcium silicate hydrate, *Cement and Concrete Research* 34 (2004) 1499 – 1519.
- [75] G.K. Sun, J.F. Young, R.J. Kirkpatrick, The role of Al in C-S-H: NMR, XRD, and compositional results for precipitated samples, *Cement and Concrete Research* 36 (2006) 18 – 29.

- [76] M.D. Andersen, H.J. Jakobsen, J. Skibsted, A new aluminium-hydrate species in hydrated Portland cements characterized by ^{27}Al and ^{29}Si MAS NMR spectroscopy, *Cement and Concrete Research* 36 (2006) 3 – 17.
- [77] P. Faucon, A. Delagrave, J.C. Petit, C. Richet, J.M. Marchand, H. Zanni, Aluminum incorporation in calcium silicate hydrates (C-S-H) depending on the Ca/Si ratio, *J. Phys. Chem. B* 103 (1999) 7796 – 7802.
- [78] H.F.W. Taylor, Sulphate reactions in concrete – microstructural and chemical aspects, *Cement Technology*, in: E.M. Gartner, H. Uchikawa (Eds.), *Ceram. Trans. Vol. 40*, American Ceramic Society, Westerville, OH, USA, 1994, pp. 61 – 78.
- [79] F. Bank, J. Schneider, M.A. Cincotto, H. Panepucci, Characterization by multinuclear high-resolution NMR of hydration products in activated blast-furnace slag pastes, *Journal of the American Ceramic Society* 86 (2003) 1712 – 1719.
- [80] M.D. Andersen, H.J. Jakobsen, J. Skibsted, Characterization of the α - β phase transition in Friedels salt ($\text{Ca}_2\text{Al}(\text{OH})_6\text{Cl}\cdot 2\text{H}_2\text{O}$) by variable-temperature ^{27}Al MAS NMR spectroscopy, *Journal of Physical Chemistry A* 106 (2002) 6676 – 6682.
- [81] O.M. Jensen, M.S.H. Korzen, H.J. Jakobsen, J. Skibsted, Influence of cement constitution and temperature on chloride binding in cement paste, *Advances in Cement Research*, 12 (2000) 57 – 64.
- [82] M.R. Jones, D.E. Macphee, J.A. Chudek, G. Hunter, R. Lannegrand, R. Talero, S.N. Scrimgeour, Studies using ^{27}Al MAS NMR of AFm and AFt phases and the formation of Friedels salt, *Cement and Concrete Research* 33 (2003) 177 – 182.
- [83] R.J. Kirkpatrick, P. Yu, X. Hou, Y. Kim, Interlayer structure, anion dynamics, and phase transitions in mixed-metal layered hydroxides: variable temperature ^{35}Cl NMR spectroscopy of hydrotalcite and Ca-aluminate hydrate (hydroalumite), *American Mineralogist* 84 (1999) 1186 – 1190.
- [84] J. Rottstegge, M. Arnold, L. Herschke, G. Glasser, M. Wilhelm, H.W. Spiess, W.D. Hergeth, Solid state NMR and LVSEM studies on the hardening of latex modified tile mortar systems, *Cement and Concrete Research* 35 (2005) 2233 – 2243.
- [85] J. Rottstegge, M. Wilhelm, H.W. Spiess, Solid state NMR investigations on the role of organic admixtures on the hydration of cement paste, *Cement and Concrete Composites* 28 (2006) 417 – 426.

- [86] J. Greener, H. Peemoeller, C. Choi, R. Holly, E.J. Reardon, C.M. Hansson, M.M. Pintar, Monitoring of hydration of white cement paste with proton NMR spin-spin relaxation, *Journal of the American Ceramic Society* 83 (2000) 623 – 627.
- [87] R. Holly, E.J. Reardon, C.M. Hansson, H. Peemoeller, Proton spin-spin relaxation study of the effect of temperature on white cement hydration, *Journal of American Ceramic Society* 90 (2007) 570 – 577.
- [88] R. Holly, H. Peemoeller, M. Zhang, E.J. Reardon, C.M. Hansson, Magnetic resonance in situ study of tricalcium aluminate hydration in the presence of gypsum, *Journal of the American Ceramic Society* 89 (2006) 1022v1027.
- [89] M. Gussoni, F. Greco, F. Bonazzi, A. Vezzoli, D. Botta, G. Dotelli, I. Natali Sora, R. Pelesato, L. Zetta, ¹H NMR spin-spin relaxation and imaging in porous systems: an application to the morphological study of white Portland cement during hydration in the presence of organics, *Magnetic Resonance Imaging* 22 (2004) 877 – 889.
- [90] A. Plassais, M.-P. Pomies, N. Lequeux, J.-P. Korb, D. Petit, F. Baberon, B. Bresson, Microstructure evolution of hydrated cement pastes, *Physical Review E* 72 (2005) 041401.
- [91] P.J. McDonald, J.-P. Korb, J. Mitchell, L. Monteilhet, Surface relaxation and chemical exchange in hydrating cement pastes: A two-dimensional NMR relaxation study, *Physical Review E* 72 (2005) 011409.
- [92] P.J. McDonald, J. Mitchell, M. Mulheron, P. S. Aptaker, J.-P. Korb, L. Monteilhet, Two-dimensional correlation relaxometry studies of cement pastes performed using a new one-sided NMR magnet, *Cement and Concrete Research* 37 (2007) 303 – 309.
- [93] K. R. Brownstein, C.E. Tarr, Importance of classical diffusion in NMR studies of water in biological cells, *Physical Review A* 19 (1979) 2446 – 2453.
- [94] J.P. Korb, M. Whaley-Hodges, R.G. Bryant, Translational diffusion of liquids at surfaces of microporous materials: Theoretical analysis of field-cycling magnetic relaxation measurements, *Physical Review E* 56 (1997) 1934 – 1945.
- [95] S. Godefroy, J.-P. Korb, M. Fleury, R.G. Bryant, Surface nuclear magnetic relaxation and dynamics of water and oil in macroporous media, *Physical review E* 64 (2001) 021605.

- [96] F. Barberon, J.-P. Korb, D. Petit, V. Morin, E. Bermejo, Probing the surface area of a cement-based material by Nuclear Magnetic Relaxation dispersion, *Physical Review Letters* 90 (2003) 116103.
- [97] J.-P. Korb, L. Monteilhet, P.J. McDonald, J. Mitchell, Microstructure and texture of hydrated cement-based materials: A proton field cycling relaxometry approach, *Cement and Concrete Research* 37 (2007) 295 – 302.
- [98] K. Friedemann, F. Stallmach, J. Kärger, NMR diffusion and relaxation studies during cement hydration – a nondestructive approach for clarification of the mechanism of internal post curing of cementitious materials, *Cement and Concrete Research* 36 (2006) 817 – 826.
- [99] E.W. Hansen, H.C. Gran, E. Johannessen, Diffusion of water in cement paste probed by isotopic exchange experiments and PFG NMR, *Microporous and Mesoporous Materials* 78 (2005) 43 – 52.
- [100] N. Nestle, P. Galvosas, J. Kärger, Liquid-phase self-diffusion in hydrating cement pastes – results from NMR studies and perspectives of further research, *Cement and Concrete Research* 37 (2007) 398 – 413.
- [101] S. N. Ghosh, S. K. Handoo, Infrared and Raman spectra studies in cement and concrete (review), *Cement and Concrete Research* 10 (1980) 771-782.
- [102] S.S. Potgieter-Vermaak, J. H. Potgieter, R. Van Grieken, The application of Raman spectrometry to investigate and characterize cement, Part I: A review, *Cement and Concrete Research* 36 (2006) 656-662.
- [103] C. Dyer, B.J.E. Smith, Application of continuous extended scanning techniques to the simultaneous detection of Raman scattering and photoluminescence from calcium disilicates using visible and near IR excitation, *Journal of Raman Spectroscopy* 26 (1995) 777 – 785.
- [104] J. Bensted, Uses of Raman spectroscopy in cement chemistry, *Journal of American Ceramic Society* 59 (1976) 140 – 143.
- [105] S. Martinez-Ramirez, M. Frias, C. Domingo, Micro-Raman spectroscopy in white Portland cement hydration: long-term study at room temperature, *Journal of Raman Spectroscopy* 37 (2006) 555 – 561.
- [106] S.P. Newman, S.J. Clifford, P.V. Coveney, V. Gupta, J.D. Blanchard, F. Serafin, D. Ben-Amotz, S. Diamond, Anomalous fluorescence in near-

infrared Raman spectroscopy of cementitious materials, *Cement and Concrete Research* 35 (2005) 1620 – 1628.

[107] M. Conjeaud, H. Boyer, Some possibilities of Raman microprobe in cement chemistry, *Cement and Concrete Research* 10 (1980) 61 – 70.

[108] S. Martinez-Ramirez, S. Sanchez-Cortes, J.V. Garcia-Ramos, C. Domingo, C. Fortes, M.T. Blanco-Varela, Micro-Raman spectroscopy applied to depth profiles of carbonates formed in lime mortar, *Cement and Concrete Research* 33 (2003) 2063 – 2068.

[109] C. Gabrielli, R. Jaouhari, S. Joiret, G. Maurin, *In situ* Raman spectroscopy applied to electrochemical scaling. Determination of the structure of vaterite, *Journal of Raman Spectroscopy* 31 (2000) 497 – 501.

[110] M.M. Tlili, M. Ben Amor, C. Gabrielli, S. Joiret, G. Maurin, P. Rousseau, Characterization of CaCO₃ hydrates by micro-Raman spectroscopy, *Journal of Raman Spectroscopy* 33 (2001) 10 – 16.

[111] K. Garbev, P. Stemmermann, L. Black, C. Breen, J. Yarwood, B. Gasharova, Structural features of C-S-H(I) and its carbonation in air – A Raman spectroscopic study. Part I: Fresh Phases, *Journal of American Ceramic Society* 90 (2007) 900 – 907.

[112] L. Black, C. Breen, J. Yarwood, K. Garbev, P. Stemmermann, B. Gasharova, Structural features of C-S-H(I) and its carbonation in air – A Raman spectroscopic study. Part II: Carbonated Phases, *Journal of American Ceramic Society* 90 (2007) 900 – 907.

[113] C.-S. Deng, C. Breen, J. Yarwood, S. Habesch, J. Phipps, B. Craster, G. Maitland, Ageing of oilfield cement at high humidity: a combined FEG-ESEM and Raman microscopic investigation, *Journal of Materials Chemistry* 12 (2002) 3105 – 3112.

[114] A.R. Brough, A. Atkinson, Micro-Raman spectroscopy of thaumasite, *Cement and Concrete Research* 31 (2001) 421 – 424.

[115] S. Sahu, D.L. Exline, M.P. Nelson, Identification of thaumasite in concrete by Raman chemical imaging, *Cement and Concrete Composites* 24 (2002) 347 – 350.